Dalton Transactions

ROYAL SOCIETY OF CHEMISTRY

PAPER

View Article Online
View Journal | View Issue

Cite this: *Dalton Trans.*, 2024, **53**, 7450

Recycling primary lithium batteries using a coordination chemistry approach: recovery of lithium and manganese residues in the form of industrially important materials†

Rafał Petrus, *[a] Adrian Kowaliński [a] and Tadeusz Lis[b]

In this study, we have investigated the potential use of post-consumer primary lithium metal batteries (LMBs) commonly used in portable electronic devices to recover lithium and manganese in the form of industrially important materials. A direct reaction of lithium-containing electronic waste with a naturally sourced ester, methyl salicylate, combined with a wide range of aliphatic alcohols has been used as a general method for recovering lithium in the form of lithium aryloxides of different nuclearities $[Li(OAr)(HOMe)_2]$ (**1**), $[Li(OAr)(HOAr)]$ (**2**), $[Li(OAr)(HOEt)]_2$ (**3**), $[Li(OAr)(H_2O)]_2$ (**4**), $[Li_4(OAr)_4(EGME)_2]$ (**5**), $[Li_6(OAr)_6]$ (**6–8**) for ArOH = methyl salicylate (**1**, **2**, **4**, **6**), ethyl salicylate (**3**, **7**), 2-methoxyethyl salicylate (**5**, **8**), and EGME = 2-methoxyethanol. The hydrolysis of **7** was then used to synthesize lithium salicylate $[Li(Sal)(H_2O)]_n$ (**10**), which is an important antioxidant in the production of oils and grease. The discharged cathode material of Li–MnO_2 batteries was investigated as a source from which $LiClO_4$, Li_2CO_3, $LiMn_2O_4$, and Mn_2O_3 can be recovered by means of water–alcohol extraction or calcination. Particular emphasis was placed on the detailed characterization of all battery components and their decomposition products. LMBs were completely recycled for the first time, and materials were recovered from the cathode and the anode.

Received 3rd March 2024,
Accepted 26th March 2024

DOI: 10.1039/d4dt00648h

rsc.li/dalton

Introduction

Lithium has played a vital role in energy production and the development of new green technologies over the past few years. As much as 80% of the lithium produced worldwide is used in battery manufacturing, particularly electric cars, which need around 20–30 kg of lithium for vehicle batteries and have caused the demand to surge. Lithium is also essential for the industrial production of ceramics, glasses, lubricants, grease, polymers, and aluminum alloys. In 2022, lithium production reached 130 000 tons, while global consumption rose to 134 000 tons. During this time, the prices of battery-grade Li_2CO_3 increased from USD 12 600 to USD 37 000 per metric ton. It is estimated that by 2040, the demand for lithium will increase 40 times.[1]

Lithium reserves are limited to 98 million metric tons globally, 66% of which is cumulated in brines, 25% is present in minerals, and 8% in sedimentary rocks. Of these, economical extraction is possible only for brines, spodumene, and lepidolite. Brines are found mainly in Bolivia, Chile, Argentina, the United States, and China. The largest spodumene and lepidolite reserves are located in Australia, China, and Canada, among others.[2] The uneven distribution of worldwide lithium deposits, difficult accessibility, and low Li content make secondary resources, such as spent lithium batteries, attractive for large-scale metal recovery.[3] Lithium battery recycling processes are performed mainly for lithium-ion batteries by means of applying pyrometallurgical or hydrometallurgical methods.[4] The primary materials recycled are components containing nickel, cobalt, copper, aluminum, and steel while recycling lithium is currently expensive and, in many cases, not profitable. In general, pyrometallurgy is used in large-scale recovery of nickel and cobalt from the cathode when lithium is left in the final slag. Hydrometallurgical methods include leaching, separating metals from the solution, and recovering metals as salts, that is $NiSO_4$, $CoSO_4$, or Li_2CO_3. Usually, Li^+ is the last metal cation to be recovered from the stream by being precipitated with Na_2CO_3, where the efficiency and purity depend to a very high degree on the concentration of lithium ions in the solution.[5] The above example shows that recycling lithium

[a]*Faculty of Chemistry, Wrocław University of Science and Technology, 23 Smoluchowskiego, 50-370 Wrocław, Poland. E-mail: rafal.petrus@pwr.edu.pl*
[b]*Faculty of Chemistry, University of Wrocław, 14 F. Joliot-Curie, 50-383 Wrocław, Poland*

†Electronic supplementary information (ESI) available: X-ray crystallographic data for **1–9** (CIF); NMR, IR, and crystallographic data for **1–10**; TEM data of the cathode material and the details of LMB recycling. CCDC 2288230–2288240. For ESI and crystallographic data in CIF or other electronic format see DOI: https://doi.org/10.1039/d4dt00648h

from end-of-life products must be enhanced in order to recover large amounts of precursor materials for battery production, which would lower the need for primary raw materials and create an economic cycle.

In this study, we decided to develop a new method for recycling primary lithium batteries (LMBs) to recover industrially important materials. This type of battery includes many subtypes that use lithium as the negative electrode, comprising various cathodes and electrolytes. The compounds usually employed as the cathode material include MnO_2, FeS_2, FeS, SO_2, $(CF)_x$, $SOCl_2$, $SOCl_2$/BrCl, SO_2Cl_2, I_2, Ag_2CrO_4, CuO, $FePO_4$, $Ag_2V_4O_{11}$, $Cu_4O(PO_4)_2$, and $Bi_2Pb_2O_5$, which are electroactive liquid or solid components that undergo reduction and lithiation during discharge. LMBs can produce voltages of 1.5 to 3.8 V depending on the type and chemical composition. Some of them, such as Li–Ag_2CrO_4, Li–$Ag_2V_4O_{11}$, or Li–I_2, have advanced medical applications, *i.e.*, in implantable defibrillators, neurostimulators, and drug infusion systems. Others, such as Li–$(CF)_x$ or high-current Li–$SOCl_2$, have aerospace or military applications. The most commonly used is Li–MnO_2, accounting for about 80% of the non-rechargeable lithium battery market. It is suitable for low-drain, long-life, and low-cost applications in portable consumer electronic devices, telecommunication, metering, instrumentation, safety/security systems, automotive, automation, office, and other equipment. These cells offer a long operating life (10 to 20 years), superior shelf life (self-discharge less than 1% per year), high cell voltage (operating voltage of 2.8–3.2 V), high energy density (up to 400 W h kg^{-1}), excellent safety and a wide operating temperature range (from −30 °C to +75 °C). Another example is cylindrical Li–FeS_2 batteries, mainly used in digital cameras as a replacement for alkaline batteries with a nominal voltage of 1.5 V.

The main challenge in recycling LMBs is the high reactivity of metallic lithium with water, forming LiOH and H_2 (1.6 dm^3 of H_2 per kg Li) with high energy release (~32 MJ per kg Li). Therefore, special safety precautions should be taken to deactivate metallic lithium, such as cryogenic treatment, mechanical crushing under an inert atmosphere, or thermal oxidation of Li, before separating battery components.[6]

The method for recycling various lithium batteries patented by TOXCO involves crushing cryogenically cooled batteries followed by hydrolysis in an alkaline solution. Separated lithium salts (Li_2SO_3, LiCl, Li_2CO_3) are refined by means of subsequent dissolution in H_2SO_4 and passed through an electrolytic membrane to form LiOH. The resulting LiOH is then dried or converted to Li_2CO_3 by adding CO_2.[7] Another patent suggests that before the reaction with H_2O and CO_2, lithium batteries should be crushed in an Ar and CO_2 atmosphere.[8] The reaction of spent batteries with H_2O followed by the addition of Na_2CO_3 was also investigated with the objective of isolating Li_2CO_3.[9] In yet another solution, it is claimed that LiOH and $LiBF_4$ can be recovered by means of cutting cylindrical lithium batteries with ultra-high pressure water in the presence/absence of fluorine inert organic solvents. Next, LiOH is obtained by precipitation from methanol and filtrate distillation. The recovered LiOH is purified with HCl to form LiCl, which is then dehydrated and dried.[10] Water is also used as a reagent for recovering the lithium battery anode material in the form of slurry.[11] Another known solution involves heating post-consumer lithium batteries under an Ar atmosphere at a temperature of 300–600 °C for 2 hours to obtain a powder containing 3–5% lithium.[12] Scrosati *et al.* reported the recycling of the anode in the form of Li_2CO_3 by reacting it with H_2O/i-BuOH, and then CO_2, as well as the recycling of the cathode material in the form of $MnSO_4$ by reacting it with H_2SO_4.[13] Another technology reports the synthesis of lithium C4–C6 alcoholates that are further hydrolyzed and reacted with Na_2CO_3, leading to Li_2CO_3.[14]

Developing safe, inexpensive, and efficient methods for recycling metallic lithium-containing batteries with a maximum recovery of all components, ensuring their conversion into value-added compounds, is particularly important for future industrial applications.

The direct reaction of LMBs with methyl salicylate in an alcohol solution has been used as a general method for reducing the thermal effect and the risk of explosion in lithium-containing waste disposal, leading to the recovery of lithium in the form of lithium aryloxides. Lithium aryloxides have numerous practical applications in organic, polymer, and materials chemistries. They have been used as precursors for lithium-containing layers,[15] oxide materials,[16] or glass-ceramics,[17] as catalysts or reagents in organic synthesis,[18–21] and as initiators in the polymerizations of lactones[22–28] and acrylamides.[29] In the electroluminescence application, lithium aryloxo derivatives have been investigated as a promising emitter[30] or interfacial material for the electron-transporting[31] and electron-injecting layers[32–34] in organic light-emitting diodes.

This paper provides a report on the synthesis of lithium aryloxides with different nuclearities $[Li(OAr)(HOMe)_2]$ (**1**), $[Li(OAr)(HOAr)]$ (**2**), $[Li(OAr)(HOEt)]_2$ (**3**), $[Li(OAr)(H_2O)]_2$ (**4**), $[Li_4(OAr)_4(EGME)_2]$ (**5**), and $[Li_6(OAr)_6]$ (**6–8**) where ArOH = methyl salicylate (**1**, **2**, **4**, **6**), ethyl salicylate (**3**, **7**), 2-methoxyethyl salicylate (**5**, **8**), and EGME = 2-methoxyethanol using lithium residues from spent LMBs. The hydrolysis of **7** was then used to synthesize lithium salicylate $[Li(Sal)(H_2O)]_n$ (**10**), which is a luminescent material or an antioxidant of grease. A method for recovering industrially important lithium and manganese from the discharged cathode material in the form of $LiClO_4$, Li_2CO_3, $LiMn_2O_4$, and Mn_2O_3 was developed. For the first time, spectroscopic, PXRD, and TEM identification of all components of LMBs and their decomposition products was performed.

Results and discussion

Synthesis of Li aryloxides by chemical recycling of primary lithium batteries

The direct reaction of lithium batteries with methyl salicylate (ArOH) in an alcohol solution has been used as a general method for disposing of metallic lithium residues in post-con-

sumer electronic waste. The use of liquid, high-boiling, and natural-origin aromatic ligands, such as methyl salicylate, for the purpose of recovering lithium anode materials in the form of lithium aryloxides was necessary to separate lithium compounds from other battery components effectively. Methyl salicylate is the main component of wintergreen oil and occurs in small amounts in essential oils and fruits. It is used as a fragrance or flavoring agent in food, beverages, and liniments, or as a mild antiseptic in oral hygiene products.[35] The high boiling point of 220 °C of methyl salicylate prevents metallic lithium from reacting with hydrophilic reagents in a violent, spontaneous, and uncontrolled manner.

We started our experiments with the most common lithium battery type, Li–MnO_2, derived from an electronic waste collection point (Fig. 1a). This type of lithium battery uses metallic Li as the anode (Fig. 1b), MnO_2 as the cathode, and $LiClO_4$ dissolved in an organic solvent (dimethoxyethane and propylene carbonate) as the electrolyte. Commercial products have different initial Li contents depending on the battery cell size. For example, according to the product data sheet, a CR2430 battery contains 0.075–0.09 g, CR2032 0.057–0.07 g, CR2025 0.048 g, and CR2016 0.023–0.03 g of Li.

In addition, the obtained lithium aryloxides show excellent solubility in conventional alcohols, which allows them to be separated from steel/plastic elements, electrolyte solvents, and cathode materials (Fig. 1c–f). In a typical reaction, 16 to 26 lithium batteries of four different types CR-2430, 2032, 2025, and 2016 were opened, and their caps with anode were placed in a round bottom flask under an atmosphere of N_2 and reacted with an excess of ArOH (Fig. 1a–d). The resulting oily liquids were dissolved in an excess of an alcohol selected from MeOH, EtOH (anhydrous or hydrous), and 2-methoxyethanol (EGME), then filtered and allowed to crystallize at −20 to 2 °C. EGME is industrially used as a solvent for resins, dyes, and quick-drying varnishes, but its applications should be avoided because it is a possible human teratogen.[36] In this work, EGME was used as an *O*,*O*′-bidentate ligand because of the easy crystallization of EGME-solvated aryloxides. The general route for synthesizing metal aryloxides by means of recycling lithium batteries is summarized in Scheme 1.

The residues of lithium anodes from Li–MnO_2 batteries have been used as an attractive reagent to synthesize a wide range of molecular materials in the form of lithium aryloxide aggregates of varying nuclearities solvated by alcohol or water molecules. Post-consumer Li–MnO_2 batteries, apart from metallic lithium residues, also contain varying amounts of Li_2CO_3, which is formed during long-term storage due to the reaction of Li with CO_2 and atmospheric moisture and the decomposition of the ether or carbonate-based electrolytes. Since the batteries have different levels of wear, the yield of the synthesized lithium aryloxides strongly depends on the metallic lithium content in the e-waste used. The yield of the isolated products was calculated on the initial Li content in the batteries declared in the product technical data sheet.[37]

The type of alcohol used to solubilize lithium aryloxides derived from battery anodes is an important parameter that

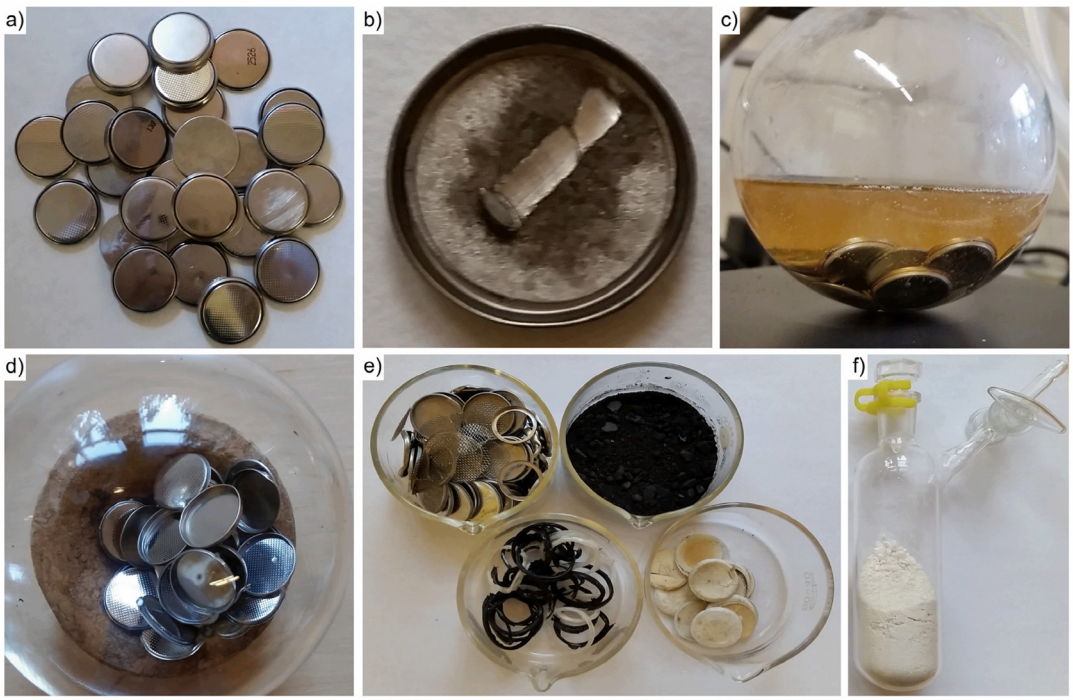

Fig. 1 Post-consumer Li–MnO_2 batteries used for synthesizing lithium aryloxides (a); coin cell cap with the lithium anode (b); reaction mixture (c); anode caps after the reaction (d); stainless steel, plastic, and cathode material recovered from the reaction (e); and isolated crystalline lithium aryloxide $[Li_6(OAr)_6]$ (f).

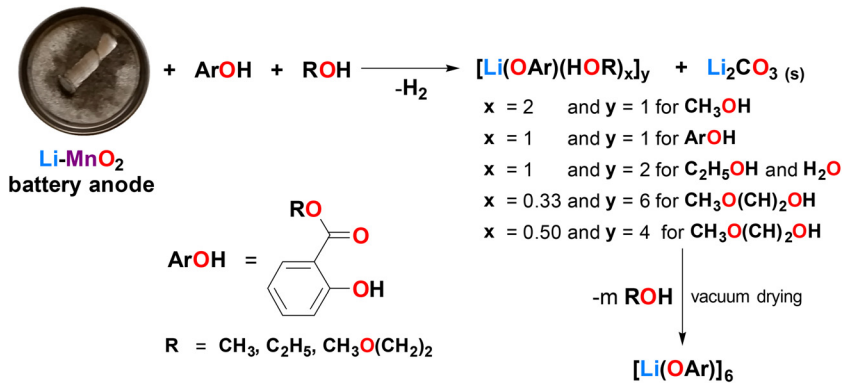

Scheme 1 The general route for the synthesis of metal aryloxides from lithium batteries.

controls the nuclearity of the resulting compounds. For example, the use of MeOH led to monomeric [Li(OAr)(HOMe)$_2$] (**1**, from 7.3 to 41.4%). The same structural motif was also observed in [Li(OAr)(HOAr)] (**2**, 20.4%), which was synthesized using an excess of ArOH over the lithium anode material. Solid-state **1** exists in two polymorphic forms, which crystallize in the orthorhombic or monoclinic system. We have previously published orthorhombic polymorph **1** and monoclinic polymorph **2**; however, since much better structures were determined for both, they are included in this paper.[38] The reaction carried out with anhydrous EtOH at −30 °C resulted in dinuclear [Li(OAr)(HOEt)]$_2$ (**3**, 26.5%). When **3** was exposed to air moisture, the quantitative formation of [Li(OAr)(H$_2$O)]$_2$ (**4**) was observed by replacing EtOH coordinated to Li centers with H$_2$O molecules. Compound **4** was received in the form of monoclinic and triclinic polymorphs. Using alcohol other than MeOH to solubilize lithium aryloxides usually produces lithium compounds that contain fully or partially esterified ligands. During heating and vacuum drying of [Li(OAr)(ROH)$_x$]$_y$, the methyl salicylate ligand is transesterified to ethyl salicylate or 2-methoxyethyl salicylate. The reaction carried out with EGME gave tetranuclear [Li$_4$(OAr)$_4$(EGME)$_2$] (**5**, 31.7%). The molecular structures of **1**–**5** are shown in Fig. 2–6.

Usually, lithium aryloxides occur as various aggregates whose structures result from the coordination ability and steric or electronic effects of ligands, as well as the donor solvent basicity and solvation effects.

Compounds **1** and **2** are based on the same structural motif, in which the Li1 atom coordinated by the chelating methyl salicylate ligand is solvated by two oxygen donor atoms of two MeOH or one ArOH molecule (Fig. 2 and 3). In Li$_2$(μ-O)$_2$ diamond core complexes **3** and **4**, Li centers bridged by two aryloxy oxygen atoms are additionally coordinated by carbonyl oxygen atoms and EtOH or H$_2$O oxygen atoms (Fig. 4 and 5). The formation of low aggregated, solvated mono- or dinuclear lithium aryloxides [Li(OAr)(solv)$_x$] is relatively limited. Monomeric lithium aryloxides are obtained when steric mono- or poly-phenolato ligands are used in the presence of strong donor solvents (ethers, amines, alcohols).[39–45] Dinuclear lithium aryloxides are usually formed using bulk phenolato

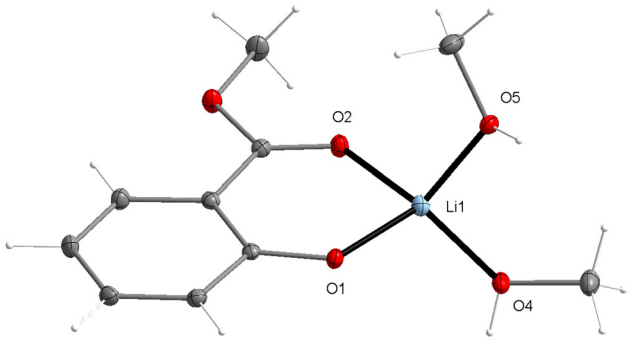

Fig. 2 The molecular structure of [Li(OAr)(HOMe)$_2$] (**1**) (for ArOH = methyl salicylate). The displacement ellipsoids are drawn at the 25% probability level.

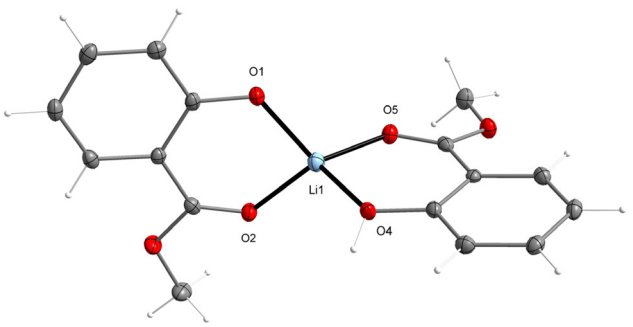

Fig. 3 The molecular structure of [Li(OAr)(HOAr)] (**2**) (for ArOH = methyl salicylate). The displacement ellipsoids are drawn at the 30% probability level.

ligands, *i.e.*, [Li$_2$(OAr)$_2$X$_2$] where ArO$^-$ = 2,6-di-*t*-butyl-4-methylphenolato,[46,47] 2,6-di-*t*-butylphenolato,[48,49] 2,6-dibenzylphenolato,[50] 2,6-di-*t*-butylphenolato,[51] 3,6-di-*t*-butyl-1-(isoquinolin-1-yl)-2-naphtholato-*N*,*O*,*O*,[52] and 1,1,7,7-tetraethyl-3,3,5,5-tetramethyl-1,2,3,5,6,7-hexahydro-*s*-indacen-4-olato,[53] and X = Et$_2$O, THF, DME, and DMSO; or Mannich,[54–56] and Schiff base ligands.[57–59] Only three lithium phenolate dimers [Li$_2$(OAr)$_2$(H$_2$O)$_x$] (where ArO$^-$ = 2-bromophenolato and x = 4;

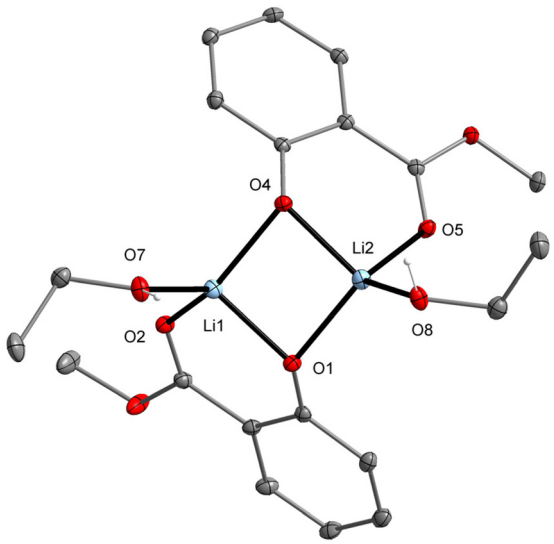

Fig. 4 The molecular structure of $[Li(OAr)(HOEt)]_2$ (**3**) (for ArOH = methyl salicylate). The displacement ellipsoids are drawn at the 25% probability level. Hydrogen atoms have been omitted for the sake of clarity.

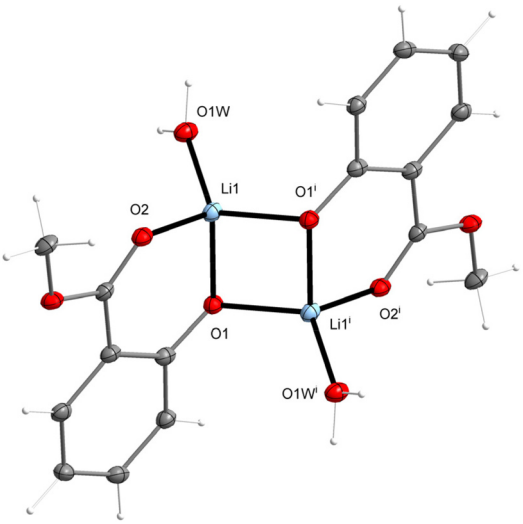

Fig. 5 The molecular structure of $[Li(OAr)(H_2O)]_2$ (**4**) (for ArOH = methyl salicylate). The displacement ellipsoids are drawn at the 25% probability level [symmetry code: (i) $-x + 1, -y + 1, -z + 1$].

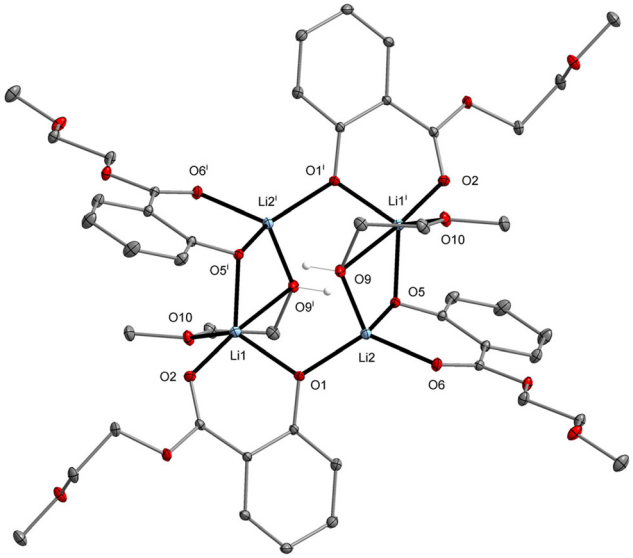

Fig. 6 The molecular structure of $[Li_4(OAr)_4(EGME)_2]$ (**5**) (for ArOH = 2-methoxyethyl salicylate). The displacement ellipsoids are drawn at the 25% probability level. Hydrogen atoms are omitted for clarity [symmetry code: (i) $-x + 1, -y + 1, -z + 1$].

2,4,6-trinitrophenolato and $x = 2$),[60,61] and $[Li_2(OAr)_2(H_2O)_2]_n$ (where ArO^- = 1-oxo-1*H*-phenalen-9-olato),[62] containing Li coordinated with H_2O in a similar manner to that in **4** have been reported. The cyclic tetranuclear $Li_4(\mu\text{-}O)_4$ core structure of **5** is uncommon (Fig. 6), and so far, it was observed only in $[Li_4(OAr)_4(H_2O)_4]$ (for ArO^- = 1,1,1-trifluoro-4-oxo-4-(pyridin-4-yl)but-2-en-2-olato).[63] Continuous-shape measurements (CShM)[64] of the coordination environment around lithium centers in **1–5** revealed the presence of the lowest departure from the ideal tetrahedral geometry for **1** then in **4** and **5** with the shape parameters S(T-4) = 0.774–0.945 (**1**), 1.216–1293 (**4**), and 1.349–1.539 (**5**). For the LiO_4 tetrahedra in **2** and **3**, the corresponding metric parameters of 3.116 for **2** and 2.520–2.616 for **3** suggest the presence of more significant geometric distortions (ESI, Table S2†).

The alcohol molecules in crystalline **1**, **3**, and **5** are very weakly coordinated to lithium ions and dissociate in solution with the generation of hexanuclear $[Li_6(OAr)_6]$ (ArOH = methyl salicylate (**6**), ethyl salicylate (**7**), and 2-methoxyethyl salicylate (**8**)), and free MeOH, EtOH or EGME (Fig. 7, 8 and ESI, Fig. S1†). Due to the similar structures, compounds **6–8** can co-crystallize together to form cocrystals. For example, compound $[Li_6(OAr)_6]$ (**7a**, ArOH = methyl salicylate (0.5), ethyl salicylate (0.5)), is formed by means of cocrystallization of **6** with **7** (ESI, Fig. S2†).

We were unable to obtain crystals of compound **8** for X-ray studies; however, compound $[Li_6(OAr)_6(EGME)_2]$ (**9**) is a molecular model that illustrates the structure of compound **8** in the form of an EMG solvate (Fig. 8). Formally, **9** can be considered a cocrystal of {**6**·**8**}·2EMG, (for ArOH = methyl salicylate (0.73), 2-methoxyethyl salicylate (0.27), Fig. 8). Compound **9** was isolated with a yield of several crystals during the synthesis of **5**. The crystal structure of **9** can also be used to visualize the initial stage of the transesterification reaction that occurs in the reaction mixture after the addition of EMG.

The coordination of C═O groups of methyl salicylate ligands to Li centers in **6** increases the positive charge on the carbonyl carbon and facilitates the attack by the oxygen atom of EMG to give a tetrahedral intermediate. This form is then deprotonated and protonated in alcoholic oxygen atoms, resulting in the elimination of MeOH and the formation of 2-methoxyethyl salicylate ligands. The presence of two EMG

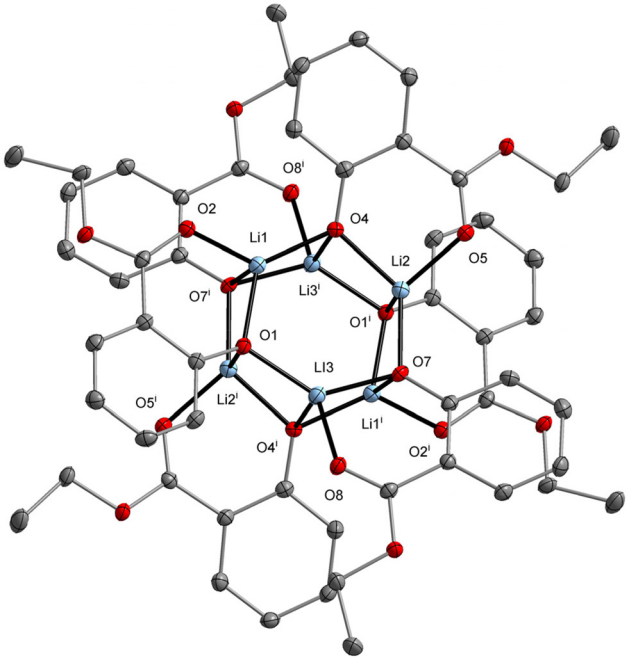

Fig. 7 The molecular structure of $[Li_6(OAr)_6]$ (**7**) (for ArOH = ethyl salicylate). The displacement ellipsoids are drawn at the 25% probability level. Hydrogen atoms are omitted for the sake of clarity [symmetry code: (i) $-x + 1, -y + 1, -z + 1$].

molecules in **9** also suggests that the Li centers mediate the nucleophilic attack of EMG on the C═O group.

Compounds **6–9** were based on a hexagonal-prismatic $Li_6(\mu_3\text{-}O)_6$ core structure comprising two Li_3O_3 units (Fig. 7, 8 and ESI, Fig. S1, S2†). This is a common structural motif in lithium coordination chemistry and has been found in $[Li_6(OR)_6]$ (RO^- = *t*-butyl 3-oxobutanoato,[65] diphenylmethanolato,[66] 2-(isopropylamino)troponato,[67] 2-methyl-1-phenylpropen-1-olato,[68] 1,1-dicyclopropylethanolato,[69] (2*S*)-1-methyl-2-(oxymethyl)pyrrolidine,[70] 1,1-dimethylprop-2-yn-oxo,[71] bis((dimethylphosphino)methyl)methanolato),[72] 2-methyl-1-(2-thienyl)propanolato,[73] dimethylbenzyloxo,[74] 2-(pyrrolidin-1-yl) ethanolato,[75] methyl 3-aminobutanoato,[76] 1-*t*-butylethenolato[77]) or $[Li_6(OAr)_6]$ (ArO^- = 2,6-dimethoxyphenolato,[78] 2-(dimethylamino)phenolato,[79] 2-methyl-8-quinolinolato[80]).

In **6–9**, Li atoms surrounded by four oxygen donor atoms adopt an axially vacant trigonal bipyramidal (**6**) or tetrahedral coordination environment (**6–9**). The CShM analysis of hexanuclear **6–7a** revealed a similar deformation in the coordination geometry around the Li atoms with shape parameters *S*(vTBPY-4) or *S*(T-4) within the range of 2.326–2.570. Due to the absence of two interplanar $Li\text{–}O_{(aryloxo)}$ bonds between Li_3O_3 rings and the formation of two additional Li–O bonds with EMG, compound **9** shows less stress within the hexagonal core and lower deformation of the tetrahedral geometry than **6–7a** (*S*(T-4) = 1.085–1.766) (ESI, Table S2†).

Compounds **1–8** have been characterized by means of ^1H, ^{13}C, and ^7Li NMR, FTIR-ATR spectroscopies and elemental analysis (ESI, Fig. S3–S26†). The diffusion-ordered NMR spectroscopy measurements confirmed the occurrence of hexanuclear compounds **6–8** and free MeOH, EtOH, EGME or H_2O in a THF-d_8 solution of **1**, **3**, **4** and **5** (ESI, Fig. S27–S33; Table S3†). The solid-state structure of **2** was preserved in solution (ESI, Fig. S28; Table S3†).

The performed reaction revealed that the type of alcohol used in combination with methyl salicylate for the reaction with battery anodes determines the nuclearity of lithium aryloxides, their solubility, and crystallization properties. Among the tested alcohols, MeOH and EtOH allowed the highest

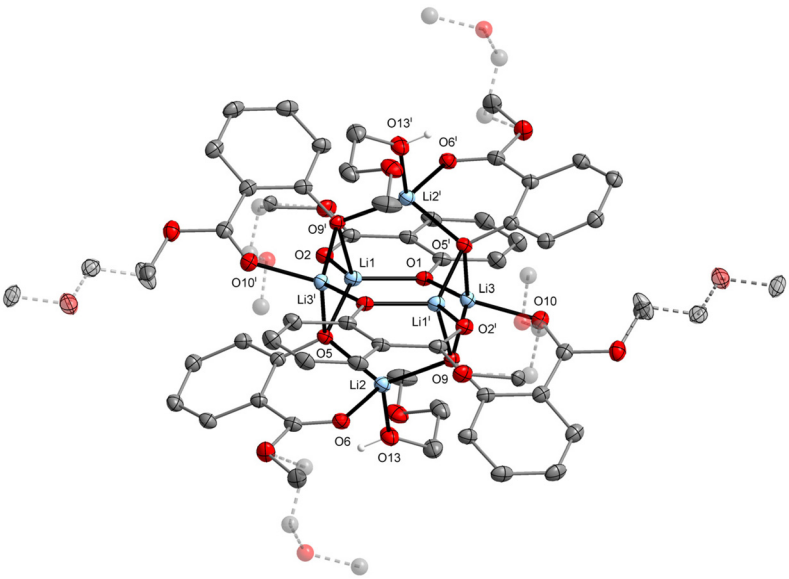

Fig. 8 The molecular structure of $[Li_6(OAr)_6(EGME)_2]$ (**9**) for ArOH = methyl salicylate (0.73) and 2-methoxyethyl salicylate (0.27). The displacement ellipsoids are drawn at the 20% probability level. Hydrogen atoms are omitted for the sake of clarity [symmetry code: (i) $-x + 1, -y + 1, -z + 1$]. The second disordered counterparts of aryloxo ligands are shown with dashed line bonds and highlighted atoms.

Table 1 Recovery of lithium from primary lithium battery anodes by reaction with methyl salicylate (ArOH) and alcohols, or H_2O (ESI, Tables S4–S12†)[a]

No.	ROH	Weight of battery (g)	Li content[b] (g)	Yield of recovery Li[c] (%)	Recovery compound[d]	Amount of recovery compound (g)
1	MeOH	78.46	1.686	14.9	**6**	5.73
2	MeOH	46.21	1.100	41.4	**6**	10.36
3	MeOH	108.5	2.085	7.3	**6**	3.46
				40.2	Li_2CO_3	4.46
4	$EtOH_{(anhydrous)}$	74.22	1.840	26.5	**7**	12.1
				30.4	Li_2CO_3	2.98
5	ArOH	69.66	1.604	20.4	**2**	14.64
6	EGME	58.66	1.431	33.7	**5**	16.71
7[e]	H_2O	70.50	1.947	18.3	$LiOH{\cdot}H_2O$	2.15
				19.4	Li_2CO_3	2.01
8	ArOH	61.37	2.04	12.3	**2**	11.2
9[f]	$EtOH_{(hydrous)}$	120.38	8.0	38.7	**4**	78.60
	$EtOH_{(hydrous)}$	120.38	8.0	32.7	**7**	64.80

[a] General conditions: lithium anodes from the post-consumer Li–MnO_2 or Li–FeS_2 batteries, methyl salicylate (ArOH), Li : ArOH = 2 : 1; excess ROH = MeOH, EtOH, EGME, and ArOH; round-bottom flask with a capacity of 100–500 mL; N_2 atmosphere; reactions performed using anodes from Li–MnO_2 batteries (entries 1–8) or FeS_2 batteries (entry 9). [b] Initial lithium content in batteries estimated using the product safety data sheet. [c] The yield of lithium recovery from discharged batteries is calculated based on the initial lithium content in the LMBs. [d] Li_2CO_3 was recovered from the anode and cathode material. [e] Reaction was performed only in H_2O without using ArOH. [f] Lithium was initially recovered in the form of **4**; next, by means of heating and vacuum drying from EtOH solution, **4** was transformed into **7**.

recovery efficiencies to be achieved due to the easy crystallization of the obtained lithium aryloxides at low temperatures (Table 1). The amount of isolated **1–9** together with Li_2CO_3 should be considered for the quantitative recovery of lithium from LMBs (ESI, Tables S4–S10†). Significant amounts of Li_2CO_3 are found in the cathode material, from which it is extracted using an H_2O/MeOH mixture. The recovery of lithium from LMBs in the form of lithium aryloxides (**2** and **4–7**) and Li_2CO_3 or $LiOH{\cdot}H_2O$ is summarized in Table 1. For example, when the yield of **6** was 7.3%, the amount of Li_2CO_3 isolated was up to 40.2% (Table 1, entry 3; ESI, Table S6†). When the yield of **7** was 26.5%, the corresponding yield of Li_2CO_3 was 30.4% (Table 1, entry 4; ESI, Table S8†). To compare the efficiency of the above results, we also exposed the anode material to H_2O at low temperatures, recovering 18.3% lithium as $LiOH{\cdot}H_2O$ and 19.4% as Li_2CO_3 (Table 1, entry 7; ESI, Table S10†). The results presented in Table 1 show that Li recovery in the form of lithium aryloxides/$LiOH{\cdot}H_2O$ and Li_2CO_3 ranges from 37.7 to 56.9% (Table 1, entries 3, 4, and 7). These products result from the decomposition of the anode material by reaction with CO_2 or electrolyte solvents during prolonged storage or by reacting with ArOH/H_2O. At this point, it is worth highlighting that in the form of **1–9**, we can recover only lithium that has not undergone an electrochemical reaction with MnO_2 through the developed recycling method. Most lithium batteries left at the electronic waste collection point were discharged in the 43 to 62% range. Analyzing the results of the recovery efficiency of Li only in the form of lithium aryloxides, we noticed that the amount of metallic Li in the anodes ranges from 7.3 to 41.4% (Table 1, entries 1–6).

The information provided above indicates the danger of storing post-consumer Li–MnO_2 batteries due to the high content of still reactive metallic lithium.

However, the high content of metallic lithium in batteries, for which an industrial recycling method has not yet been developed, can be easily used to produce drugs on the black market. The reduction of ephedrine and pseudoephedrine extracted from pharmaceutical cold and allergy products to methamphetamine requires the use of anhydrous ammonia and metallic lithium from primary batteries.[81]

The high metallic lithium content in primary Li batteries can also be explained by their long service life, which can be up to several years in low-power devices. The very low electrochemical wear of batteries may be due to their lifetime being, in many cases, much longer than that of the devices they power. Analyzing the batteries used in our reaction in terms of their manufacturers, we noticed that the cheapest batteries have the lowest discharge and contain the most lithium. These findings support our suggestion that battery life is longer than that of devices powered by these batteries.

As a source of lithium for the reaction, we have also tested Li–MnO_2 CR2 or CR123A photo batteries; however, due to their high discharge, the recovery yield of lithium in the form of compound **2** was only 12.3% (Table 1, entry 8). Nevertheless, it should be noted that as much as 11.2 g of compound **2** was obtained from three post-consumer photocells.

Another attractive source of lithium is cylindrical Li–FeS_2 batteries (Fig. 9a). In this type of battery, the anode is lithium foil, the cathode is a mixture of FeS_2 with graphite and carbon black, and the electrolyte is $LiCF_3SO_3$ dissolved in a mixture of dimethoxyethane and ethylene/propylene carbonate. In our research on Li–FeS_2 battery recycling, we focus exclusively on recovering lithium from the anode material. When the anode material derived from 16 R03/AAA batteries (Fig. 9b) with a total weight of 2.96 g was reacted with ArOH and hydrous EtOH, a mixture of **4** and its partially esterified derivative **4a** was obtained in an amount of 78.6 g (38.7%, Fig. 9c and

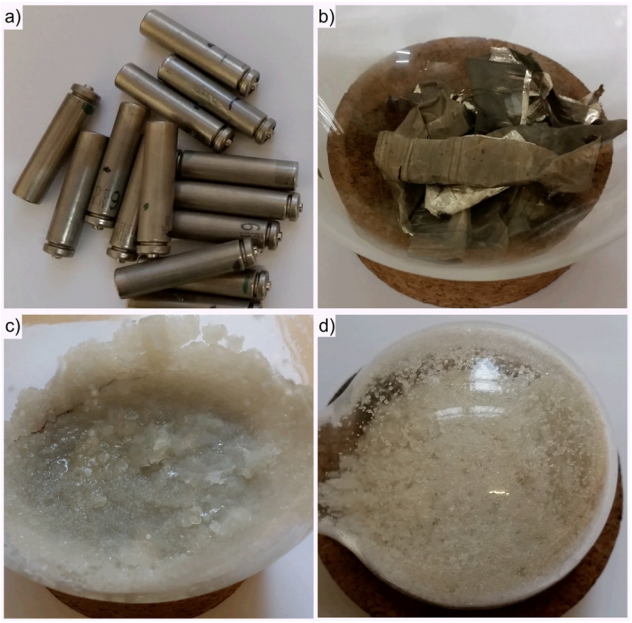

Fig. 9 Cylindrical Li–FeS_2 batteries (a), isolated lithium anode (b), and **4** and **7** isolated in the crystalline form (c and d).

Fig. S34†). By means of recrystallizing the product obtained from hydrous EtOH, followed by vacuum drying and heating, H_2O molecules were removed from the Li^+ coordination sphere, and the methyl salicylate ligand was transesterified, leading to the formation of compound **7** (32.7%) as shown in Fig. 9d (Table 1, entry 9).

An attractive alternative for converting **7** to industrially important chemicals is direct hydrolysis to lithium salicylate, an important antioxidant of lubricating oils and grease.[82] Lithium salicylate is a neuroactive lithium salt with a smoother absorption rate than Li_2CO_3.[83] It is also a promising luminescent material useful for detecting thermal neutrons.[84] The reaction of **7** with H_2O led to the isolation of a one-dimensional coordination polymer $[Li(Sal)(H_2O)]_n$ (**10**, 73%; Fig. 10; ESI, Fig. S35†). Compound **10** was previously synthesized by reacting equimolar amounts of salicylic acid and LiOH in water.[85] In **10**, Li^+ ions and water molecules form $\{Li(H_2O)\}_n$ helices, which link the carboxylate groups of the Sal ligands. The comparison of the powder diffraction pattern of **10** simulated from the crystal structure with the resulting crystalline material confirmed quantitative hydrolysis of **7** (Fig. 10).

Powder X-ray diffraction, IR, Raman and NMR spectroscopy, and TEM microscopy analysis of cathode material of Li–MnO_2 batteries

The PXRD study of the material isolated from the cathode caps of Li–MnO_2 batteries showed that it consists of crystalline graphite and Li_2CO_3 phases and poorly crystalline MnO_2, carbon black, and $Li_xMn_2O_4$ (Fig. 11a). The technical data sheet of the batteries used in this study revealed that they

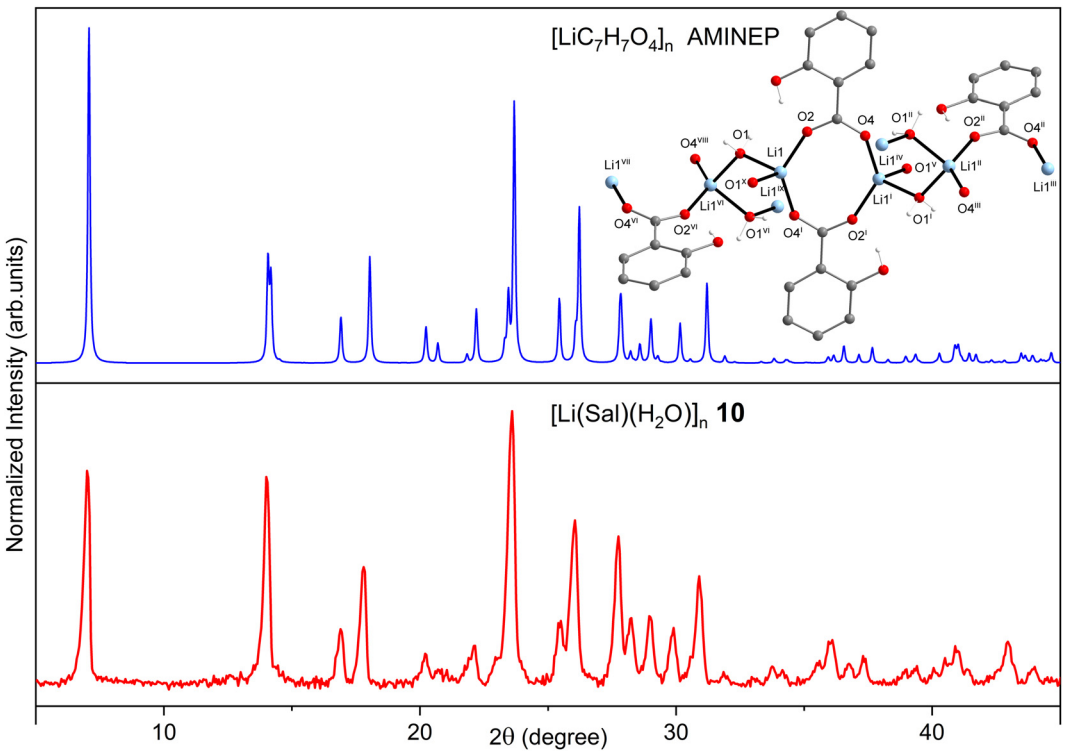

Fig. 10 Comparison of PXRD patterns of **10** with reference standards of $[Li(Sal)(H_2O)]_n$ simulated from crystal structure deposited in CCDC with refcode AMINEP. Symmetry codes (i) $1-x, -y, 2-z$; (ii) $x, -0.5-y, 0.5+z$; (iii) $1-x, -0.5+y, 2.5-z$; (iv) $1-x, -1-y, 2-z$; (v) $x, 0.5-y, 0.5+z$; (vi) $1-x, 0.5+y, 1.5-z$; (vii) $1-x, 0.5+y, 1.5-z$; (viii) $x, 0.5-y, -0.5+z$; (ix) $x, 1+y, z$; and (x) $1-x, -0.5+y, 1.5-z$.

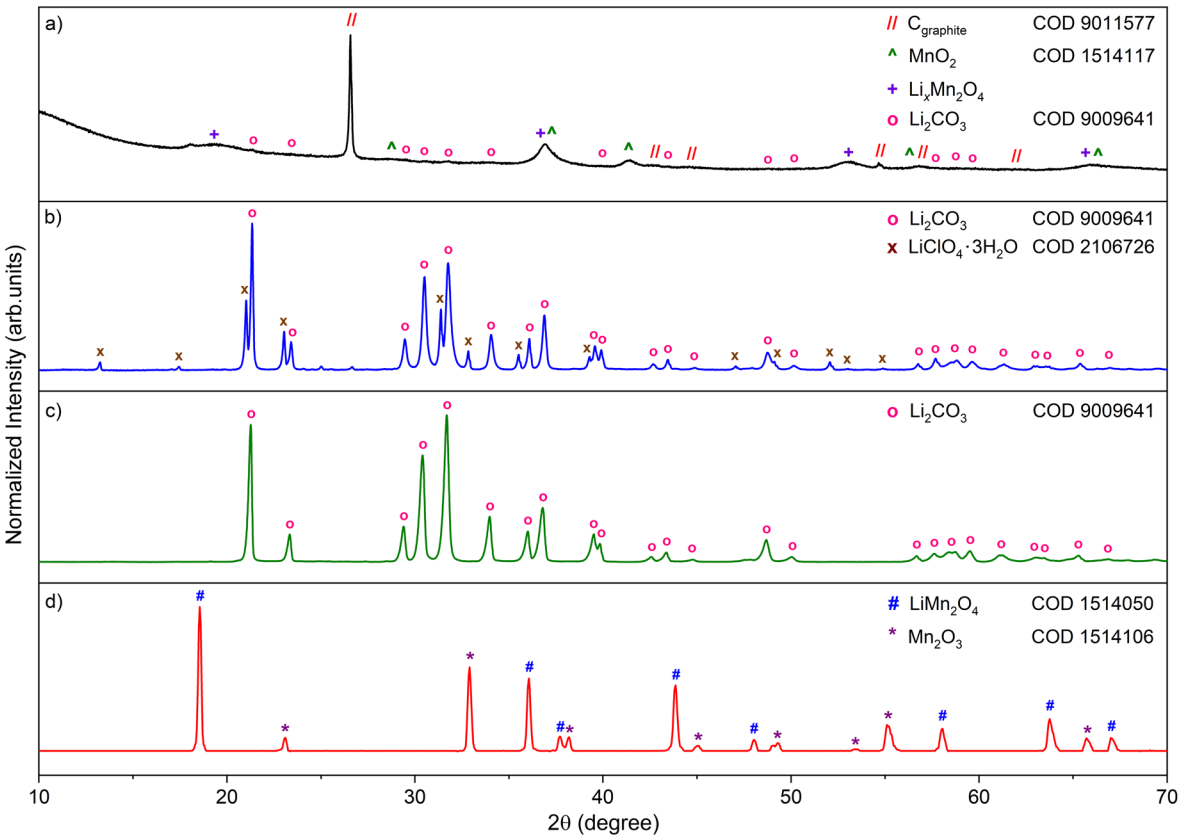

Fig. 11 PXRD patterns of the crude cathode material (a); Li_2CO_3/$LiClO_4$·$3H_2O$ mixture extracted with H_2O and MeOH treatment (b); Li_2CO_3 after purification with MeOH (c); and oxide materials received by means of calcination of cathode residues at 900 °C (d).

contain between 12 and 42 wt% of MnO_2 and between 1 and 5 wt% of graphite or its mixture with carbon black. The carbon material in the battery acts as a highly conductive or dispersing agent of MnO_2. The influence of the carbon ratio or carbon types on the structure, morphology, specific surface area, and electrochemical properties of the MnO_2/C electrodes is well known and has been previously reported for the MnO_2 composite with carbon, CNTs, or graphene.[86] Due to its relatively high discharge voltage, heat-treated electrolytic γ-MnO_2 is usually used as a positive electrode material in Li–MnO_2 cells. The γ-MnO_2 structure consists of an intergrowth of tetragonal pyrolusite β-MnO_2 in an orthogonal ramsdellite phase with varying degrees of microtwinning.[87] In battery production, heat treatment of γ-MnO_2 at 350 to 400 °C removes high moisture content and increases the concentration of β-MnO_2 in the solid material. Therefore, the β-MnO_2 polymorph is a major phase that undergoes lithiation in non-aqueous primary Li batteries.[88] The discharge process of Li–MnO_2 batteries can be considered a solid solution reaction described by the equation $MnO_2 + xLi^+ + x\bar{e} \rightarrow Li_xMnO_2$, which results in the formation of partially lithiated MnO_2 (Li_xMnO_2). During battery discharge, the structure of the cathode material changes as a result of the reduction of Mn(IV) to larger Mn(III) ions and the incorporation of Li^+ into β-MnO_2, which leads to the expansion of the lattice. During the initial discharge, Li^+ ions are randomly incorporated into β-MnO_2 without changing the crystal structure of the pyrolusite-type phase. Then, as the reduction proceeds by lithiation, the expanded β-MnO_2 undergoes a phase transition to $Li_xMn_2O_4$ ($0 \leq x \leq 2$). The crystal structure of the cathode material after complete discharge has not been definitively determined. However, based on the experimental results that involved the chemical lithiation of β-MnO_2 using ^{n}BuLi, the formation of spinel-related phase isostructural to cubic $LiMn_2O_4$ or tetragonal $Li_2Mn_2O_4$ was proposed.[89] The characteristic peak at 2θ values of 26.6° was assigned to hexagonal graphite. The analysis of the PXRD pattern shows that, except for graphite, there are wide diffraction peaks between 2θ = 20–30° and 40–45°, corresponding to the crystal planes (002) and (101) of amorphous carbon. The presence of the β-MnO_2 phase was confirmed based on the characteristic peaks at 2θ values of 36.9°, 41.3°, 42.9°, 56.8°, and 66.1° (Fig. 11a). The diffraction peaks at 2θ values of 19.2° and 52.7° in Fig. 11a were a particular characteristic of the intermediate spinel phase.[90] The same diffraction peaks were also observed in the $Li_{0.92}Mn_2O_4$ superstructure generated by thermal-pressure heating of $LiMn_2O_4$.[91] The presence of different carbon types and the chemical change of electrode materials during battery discharge finally give a mixture of carbon with β-MnO_2 and spinel $Li_xMn_2O_4$.[92] The presence of Mn(III) oxide phases of hausmannite Mn_3O_4 and α-, γ-Mn_2O_3

was excluded by the lack of agreement with the reference patterns.

The discharged cathode material generally contains between 0.01813 and 0.03128 g of Li and between 0.41026 and 0.4554 g of Mn per 1 g of solids (ESI, Tables S4–S10†). Treating the cathode material with excess cold demineralized water led to the extraction of Li_2CO_3 and $LiClO_4$ into the liquid phase. Following the evaporation of water, MeOH was added to the obtained solid, separating the mixture of $LiClO_4{\cdot}3H_2O$ and Li_2CO_3 (Fig. 11b). The insoluble phase in MeOH consists of Li_2CO_3 (Fig. 11c). The experimental path for recovering lithium salts from the cathode material of Li–MnO_2 batteries is shown in Scheme 2.

FTIR-ATR and Raman spectroscopy were employed as useful techniques for determining the phase composition of the recovered lithium salts. The IR spectrum of Li_2CO_3 (Fig. 12a) shows a band at 476 cm^{-1} attributed to quasilattice vibrations and four bands corresponding to the internal vibrations of isolated CO_3^{2-} at 1412 cm^{-1} from asymmetric stretching vibrations, at 1087 cm^{-1} from symmetric stretching vibrations, at 859 cm^{-1} from out-of-plane bending vibrations, and at 739 and 712 cm^{-1} from bending vibrations. The bands at 1459, 1090, 746, and 712 cm^{-1} are present also in the Raman spectrum, together with external lattice vibrational bands at 274, 194, 157, 128, and 97 cm^{-1} (Fig. 13a).[93] The appearance of the asymmetric stretching and rocking bands of ClO_4^- at 1071 and 623 cm^{-1} in the IR spectrum and the symmetric stretching of ClO_4^- at 936 cm^{-1} in the Raman spectrum of $LiClO_4{\cdot}3H_2O$ allows it to be distinguished from Li_2CO_3 (Fig. 12b and 13b).[94] A spectroscopy analysis was also carried out on the $Li_2CO_3/LiClO_4{\cdot}3H_2O/LiOH/LiOH{\cdot}H_2O$ mixture obtained by reacting the lithium battery anode and the cathode with distilled water. The presence of the HO^- stretching band at 3675 cm^{-1} in the FTIR spectrum is characteristic of anhydrous LiOH, while the band at 3566 cm^{-1} is typical of asymmetric stretching of H_2O in $LiClO_4{\cdot}3H_2O$ or $LiOH{\cdot}H_2O$

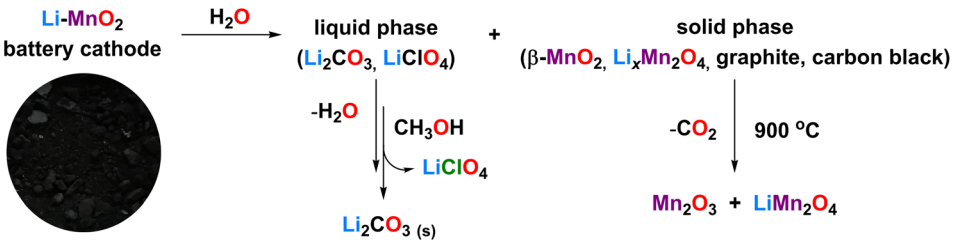

Scheme 2 Recovery of lithium salt ($LiClO_4{\cdot}3H_2O$, Li_2CO_3) and industrially important $LiMn_2O_4$ and Mn_2O_3 oxides from the cathode material of Li–MnO_2 batteries.

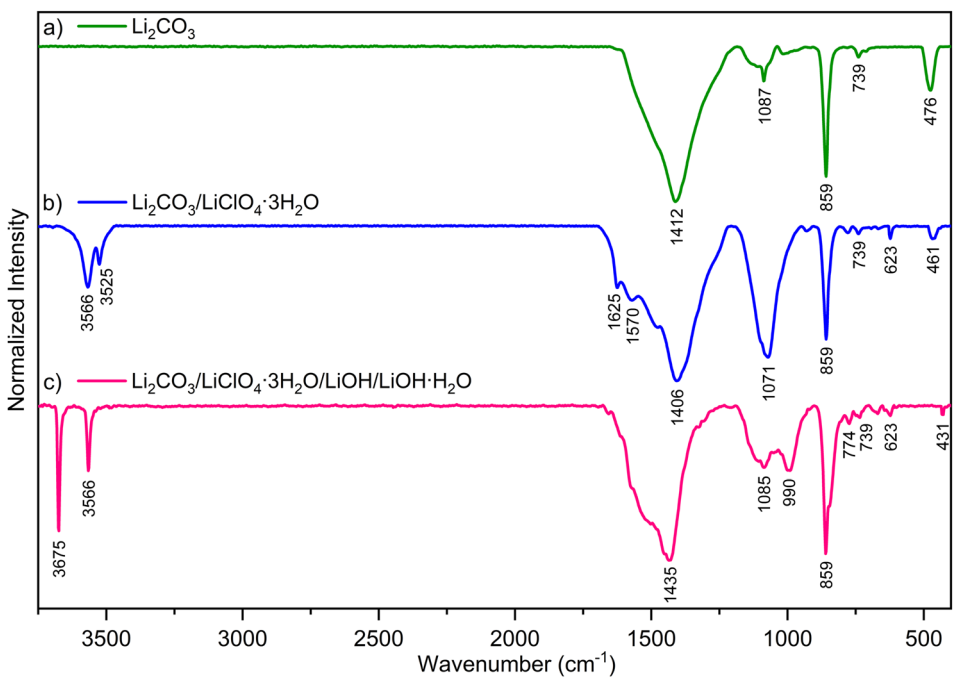

Fig. 12 FTIR-ATR spectra of lithium salts recovered from Li–MnO_2 batteries: Li_2CO_3 (a); $Li_2CO_3/LiClO_4{\cdot}3H_2O$ (b); and $Li_2CO_3/LiClO_4{\cdot}3H_2O/LiOH/LiOH{\cdot}H_2O$ (c).

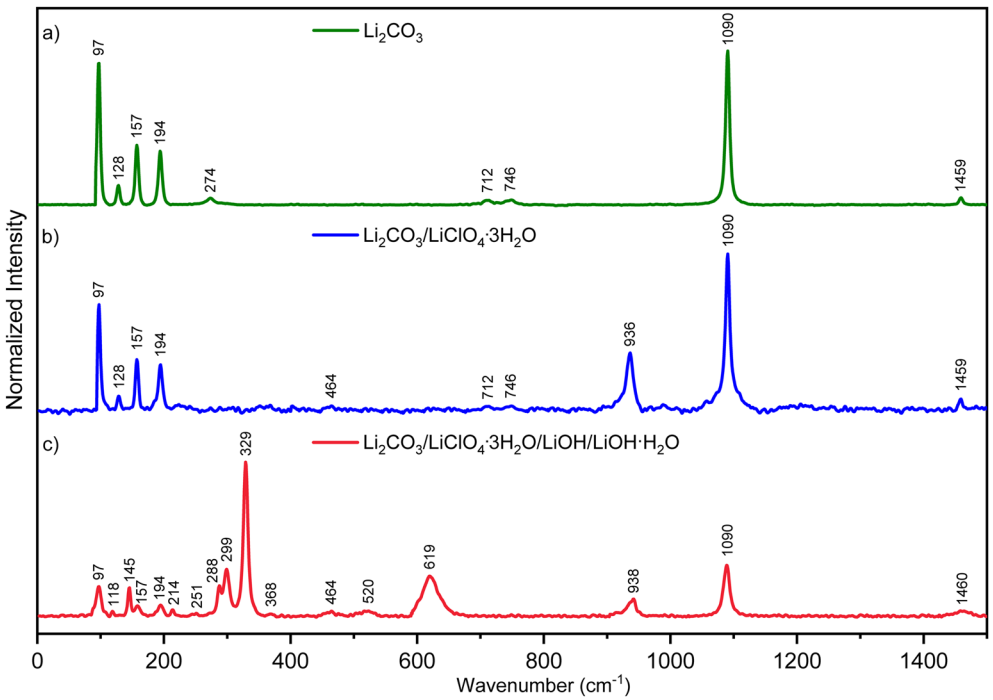

Fig. 13 Raman spectra of lithium salts recovered from Li–MnO_2 batteries: Li_2CO_3 (a); $Li_2CO_3/LiClO_4{\cdot}3H_2O$ (b); and $Li_2CO_3/LiClO_4{\cdot}3H_2O$/LiOH/$LiOH{\cdot}H_2O$ (c).

(Fig. 13c).[95] The $LiClO_4{\cdot}3H_2O$ phase was elucidated using Raman spectroscopy based on the presence of symmetric stretching and scissoring bands of ClO_4^- at 936 and 464 cm^{-1} (Fig. 13c). The band at 619 cm^{-1} and 331 cm^{-1} was assigned to the translational vibration and A_{1g} mode of LiOH.[96,97] However, they are observed only in the spectra of LiOH contaminated by Li_2CO_3 or other lithium salts.[98,99] The HO^- or lattice translations at 299, 288, 214, 157, and 118 cm^{-1} are typical of LiOH. The low-intensity bands at 520, 368, and 251 cm^{-1} arise from $LiOH{\cdot}H_2O$ (Fig. 13c).[100,101]

^{7}Li NMR studies in D_2O of three before-investigated lithium salt compositions revealed only one chemical shift at 2.86 ppm for solvent-separated ions (ESI, Fig. S36†). The ^{1}H NMR analysis of organic fractions in D_2O obtained after the separation

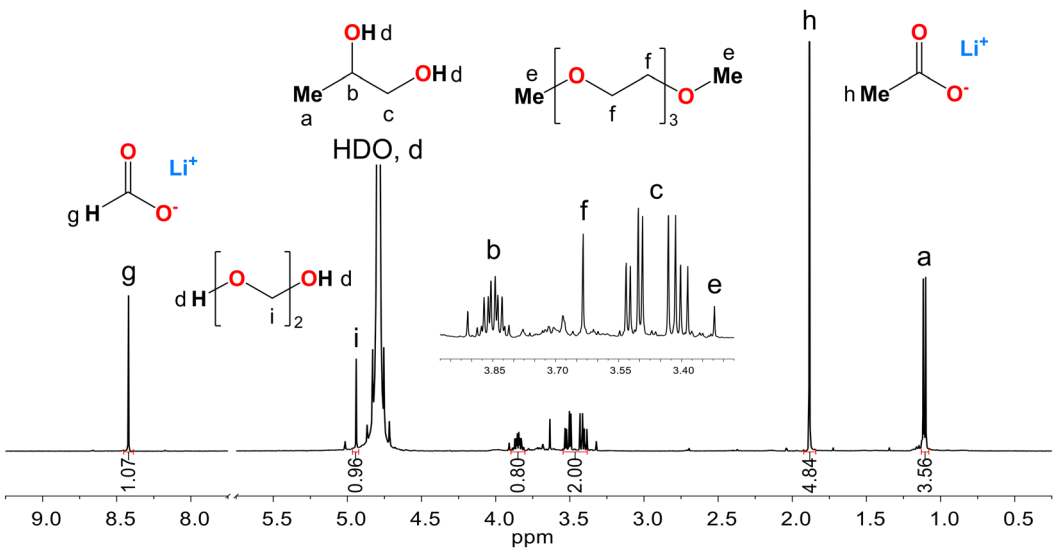

Fig. 14 ^{1}H NMR spectrum in D_2O of electrolyte solvents decomposition products: HCOOLi, CH_3COOLi, 1,2-propanediol and triethylene glycol dimethyl ether.

of $LiClO_4 \cdot 3H_2O$ and Li_2CO_3 contains decomposition products of electrolyte solvents, *i.e.*, 1,2-propanediol, triethylene glycol dimethyl ether, and lithium carboxylates.

The presence of HCOOLi and CH_3COOLi was confirmed based on the characteristic resonance signal of the HCO or CH_3CO groups at 8.42 ppm and 1.88 ppm (Fig. 14). Propylene glycol was identified by resonance signals from the CH, CH_2, and CH_3 groups at 3.85, 3.46, and 1.11 ppm, respectively. Small intensity peaks at 3.63 and 3.32 ppm arise from the CH_2 and CH_3 groups belonging to triethylene glycol dimethyl ether (Fig. 14 and ESI, Fig. S36†). At 4.94 ppm, OCH_2 groups of dimethylene glycol were observed, formed by the oxidation of MeOH and then hydrolysis of HCOH.[102] When the spectra of the electrolyte solvent residues were measured in CD_3OD, propylene glycol, and lithium carboxylates were identified as the main phases (ESI, Fig. S36†). The identified compounds were

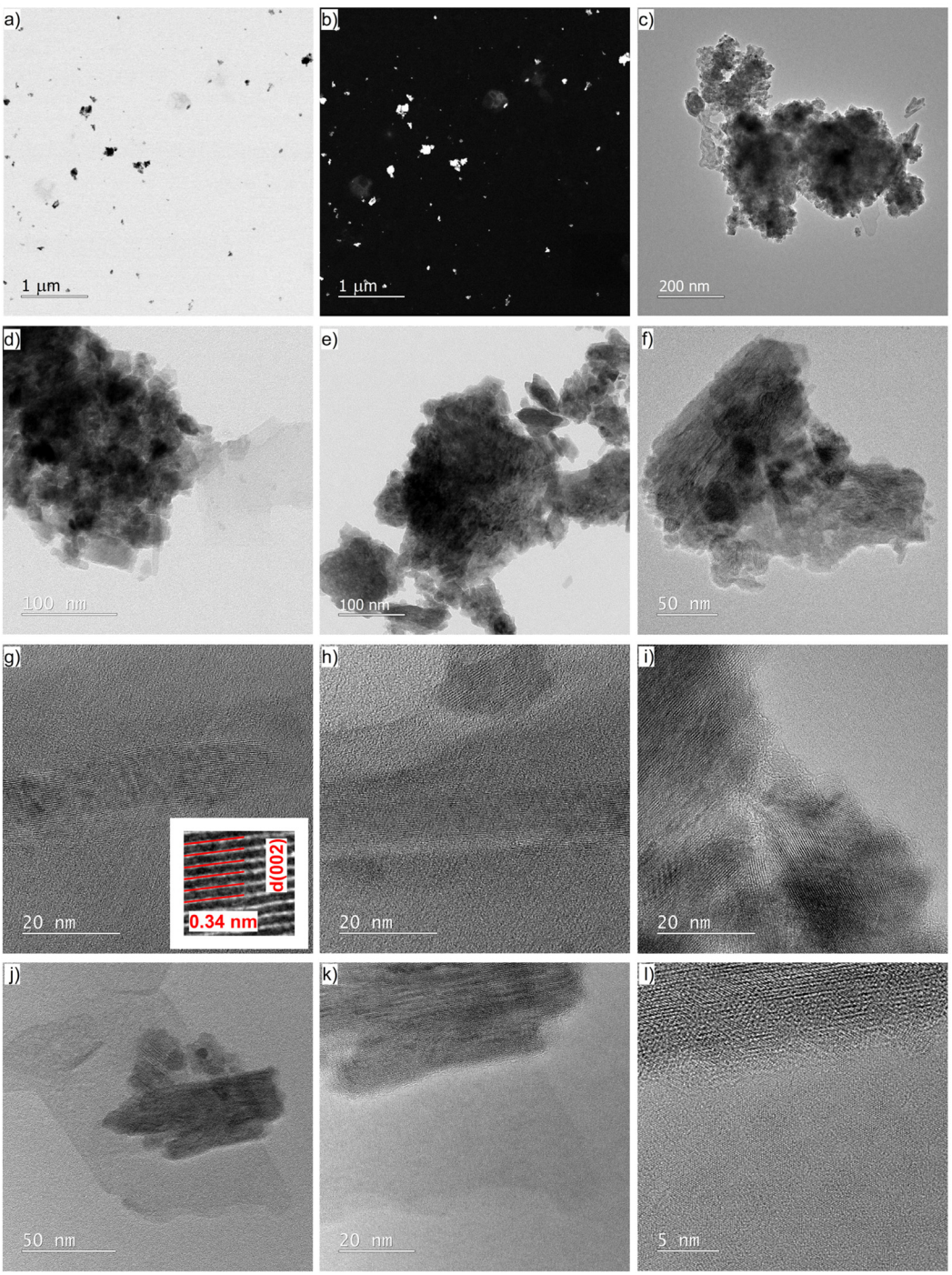

Fig. 15 TEM analysis of the discharged cathode material containing carbon black, graphite, β-MnO_2 and $Li_xMn_2O_4$ phases (a–l).

consistent with the discharge products of nonaqueous rechargeable Li–O_2 batteries containing ether and carbonate-based electrolytes.[103,104]

The morphology and composition of the carbon composite with β-MnO_2 and $Li_xMn_2O_4$ were investigated by means of transmission electron microscopy (TEM). The investigated material consists of a large number of irregularly shaped aggregates, two-dimensional sheet-like structures, and a small number of plate or rod-shaped nanocrystals, which are clumped together in a disordered manner (Fig. 15a–l). An EDS analysis of the cathode material confirms the presence of aggregates with different C:Mn:O contents, which agrees well with the mixture of phases observed by the PXRD study (ESI, Fig. S37 and S38†). An HRTEM analysis reveals the presence of a highly ordered crystalline graphite structure mixed with a small amount of amorphous carbon (Fig. 15g and h). The estimated value of the interplanar *d* spacing of 0.34 nm corresponds to the (002) planes of the hexagonal graphite structure (Fig. 15g). The graphite and amorphous carbon flakes can occur separately in the analyzed material (Fig. 15g–h, j–l) or form crystalline or partially crystalline aggregates with manganese-rich oxide phases (Fig. 15c–f). The selected area electron diffraction (SAED) pattern collected from the cathode material revealed that the sample consists of two different metal oxide phases (ESI, Fig. S39†). The first one is β-MnO_2 identified based on diffraction rings corresponding to the (110), (101), and (200) planes with estimated *d*-spacings of 0.31, 0.24, and 0.22 nm, respectively. The representative TEM micrographs of the β-MnO_2/C composite are presented in Fig. 15c–f, showing pyrolusite aggregates on the amorphous carbon sheet. A trait characteristic of β-MnO_2, is the formation of rod-shaped nanocrystals, several examples of which have been observed during the TEM analysis (ESI, Fig. S40†). The second metal oxide phase was initially identified as one of the components of multiphase aggregates; later, we also found that it forms plate nanocrystals with interplanar distances of 0.49 nm (Fig. 15i and ESI, Fig. S40†). According to the PXRD study, this crystalline product can be described as an intermediate $Li_xMn_2O_4$ spinel. Comparable *d* spacing distances were observed for cubic $Li_{0.03}Mn_2O_4$ (0.46 nm for (111)), $LiMn_2O_4$ (0.48 nm for (111)) or tetragonal $Li_{0.89}Mn_2O_{3.84}$ (0.47 nm for (101)) oxides.[105–107] The high-angle annular dark-field scanning transmission electron microscopy (HAADF-STEM) and EDS maps show plate and rod nanocrystals that are built with Mn and O elements (Fig. 16a–h). We have also found that the surface of the metal oxide particles (Fig. 16a–h) or

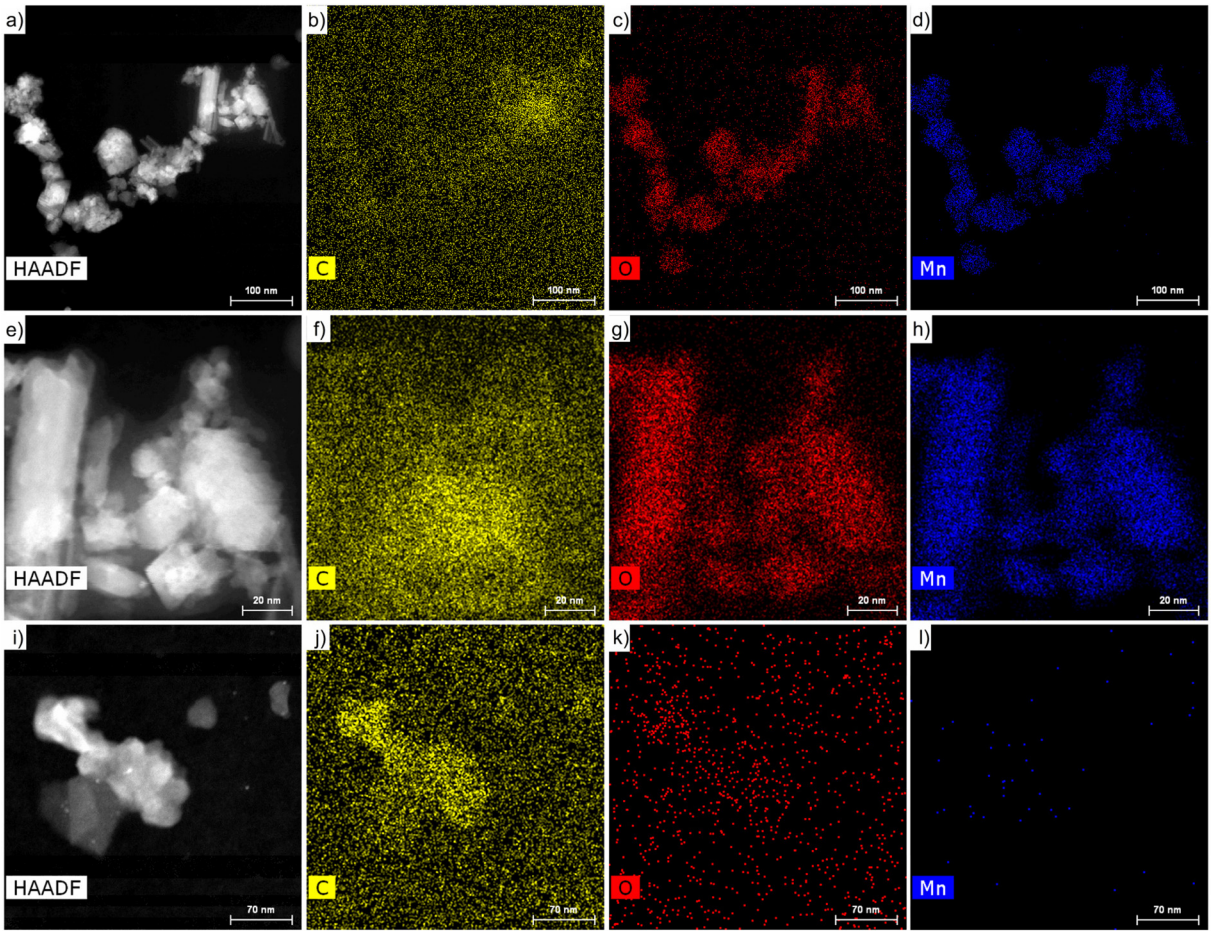

Fig. 16 HAADF-STEM and EDS maps of discharged cathode material containing carbon black, graphite, β-MnO_2 and $Li_xMn_2O_4$ phases (a–l).

crystalline graphite (Fig. 16i–l) is covered with amorphous carbon shells.

The residual cathode material was then calcined at 900 °C to remove carbon components. The weight loss caused by graphite and carbon black decomposition ranged from 11.3% to 14.3%, producing a mixture of spinel $LiMn_2O_4$ and Mn_2O_3 (bixbyite C) with small amounts of Li_2CO_3. These findings revealed that β-MnO_2 and $Li_xMn_2O_4$ discharged products transform into mixed-valence Mn(III)–Mn(IV) phases of $LiMn_2O_4$ and Mn_2O_3 by means of applying heat treatment at 900 °C. An additional 1.1 to 2.9% by weight of Li_2CO_3 was removed from the obtained solids using cold water extraction.

These values indicate that 82.8 to 87.6% by weight of the discharged cathode material can be recovered in the form of industrially important $LiMn_2O_4$ and Mn_2O_3 oxides (Fig. 11d). The general route for recovering lithium and manganese as $LiMn_2O_4$ and Mn_2O_3 oxides from the cathode material of Li–MnO_2 batteries is shown in Scheme 2.

Conclusion

In this study, we have developed a simple and efficient method for recovering lithium and manganese from spent primary lithium metal batteries (LMBs) in the form of industrially important lithium salts or homo- and heterometallic oxide materials. Compared to state-of-the-art systems, our approach provides affordable technological solutions that reduce the thermal effect and explosion hazard during the disposal of lithium-containing waste, leading to the recovery of lithium in the form of lithium aryloxides $[Li(OAr)(HOMe)_2]$ (**1**), $[Li(OAr)(HOAr)]$ (**2**), $[Li(OAr)(HOEt)]_2$ (**3**), $[Li(OAr)(H_2O)]_2$ (**4**) $[Li_4(OAr)_4(EGME)_2]$ (**5**), and $[Li_6(OAr)_6]$ (**6–8**) where ArOH = methyl salicylate (**1**, **2**, **4**, **6**), ethyl salicylate (**3**, **7**), and 2-methoxyethyl salicylate (**5**, **8**), and EGME = 2-methoxyethanol. These are attractive molecular materials with numerous potential applications in organic synthesis, polymerization of cyclic monomers, and preparation of lithium-containing oxide materials, ceramics, or glass ceramics. The yield of the synthesized lithium aryloxide strongly depends on the metallic lithium content in the e-waste used. Direct hydrolysis of **1–8** enables the synthesis of lithium salicylate $[Li(Sal)(H_2O)]_n$ (**10**), which is an important antioxidant in the production of oils and grease. We have shown that the type of alcohol used in combination with methyl salicylate determines the nuclearity of lithium aryloxides, their solubility, and crystallization properties. Among those tested, methanol and ethanol provided the highest recovery efficiencies due to the easy crystallization of the obtained lithium aryloxides at low temperatures; the choice of these cost-effective reagents contributes to overall operational savings.

We have also shown that most of the spent LMBs were discharged in the 43 to 62% range and contained a considerable amount of metallic lithium that must be neutralized before recycling. We have also established that the cathode material of spent Li–MnO_2 batteries is an attractive e-waste source for recovering $LiClO_4$, Li_2CO_3, $LiMn_2O_4$, and Mn_2O_3 by means of water–alcohol extraction or calcination. This study is the first in which particular emphasis is placed on the detailed characterization of all battery components and their decomposition products. In view of the sustainable management of natural resources, we propose the recovery of all valuables contained in spent LMBs. We believe that these results represent an important advance in recycling LMBs as a multistep process using safe and environmentally compatible operation.

Experimental section

All syntheses were performed under a dry N_2 atmosphere using standard Schlenk techniques. All chemical reagents were purchased from commercial sources: methyl salicylate, 2-methoxyethanol (Sigma Aldrich, St. Louis, MO, USA); THF-d_8, DMSO-d_6 (Deutero GmbH), MeOH, and EtOH (Carl Roth). MeOH and EtOH were distilled over Mg, and THF-d_8 was distilled over Na. Li–MnO_2 and Li–FeS_2 batteries were derived from an electronic waste collection point at the Wrocław University of Science and Technology. ^{1}H, ^{7}Li, and ^{13}C NMR spectra were recorded at room temperature with a JEOL JNM-ECZ 400 MHz spectrometer. Chemical shifts were reported in parts per million and referenced to the residual protons in deuterated solvents. The ^{7}Li spectra were referenced to a 0.1 M solution of $LiNO_3$ in D_2O. FTIR-ATR spectra were recorded with a Bruker Vertex 70 vacuum spectrometer, with a resolution of 2 cm^{-1}. The Raman spectra were measured on a MultiRAM Bruker FT-Raman spectrometer equipped with an Nd:YAG (1064 nm) laser, with a resolution of 4 cm^{-1}. Elemental analyses were performed with a PerkinElmer 2400 CHN elemental analyzer. The thermal decomposition of the cathode material was performed in atmospheric air using an NT 1313 furnace (Neotherm) equipped with a KXP4 thermostat. Battery components and their decomposition products were investigated by powder XRD using an Empyrean, PANalytical diffractometer, and the powder diffraction database COD. The morphology of cathode materials was examined using an FEI Tecnai G^2 20 X-Twin TEM microscope equipped with a field-emission gun and an integrated energy-dispersive spectrometer (EDAX) and a FEI (S)TEM Titan^3 G^2 60–300 with four EDS Super-X detectors. For (S)TEM observations, 200-mesh copper grids with lacey carbon films were used. Signals from both copper and carbon (from the grids) were observed in the TEM-EDX spectra. Single-crystal XRD data were collected using Xcalibur Ruby (**1_m**, **4_m**, **7**, **7a**), Xcalibur (**3**, **4_t**, **9**), or XtaLAB Synergy R (**1_o**, **2**, **4a**, **5**) diffractometers at 100 K.[108] The experimental details and crystal data are given in Table S1.† The structures were solved by direct methods and refined by the full-matrix least-squares method on F^2, using the SHELXTL package.[109] Non-hydrogen atoms were refined with anisotropic thermal parameters. All hydrogen atoms were positioned geometrically and added to structure factor calculations but were not refined. Molecular graphics for the resulting structures were created using Diamond (version 3.1e).[110]

CCDC 2288230–2288240 contain the supplementary crystallographic data for this paper.†

Li–MnO_2 battery recycling procedure

The procedure applied for recycling LMBs using methyl salicylate and aliphatic alcohols was as follows. Typically, 16 to 26 batteries with a weight ranging from 46.21 to 108.5 g were used in the reaction. First, Li–MnO_2 batteries were opened and separated into anode and cathode parts. Detailed information regarding the reactions performed and the type of batteries used is included in Tables S3–S10.† In the standard procedure, elements of post-consumer lithium batteries containing lithium anodes were placed into a round-bottom flask with a capacity of 500–1000 cm^3. Then, 10 to 15 cm^3 of methyl salicylate was introduced under a nitrogen atmosphere, and the reaction was carried out at 0 °C for 0.5–3 h. The obtained oily product was dissolved in 60 cm^3 of MeOH or EtOH, 30 cm^3 of EGME, and left for another 2–3 hours. The resulting reaction mixture was filtered to separate battery components and solid impurities, *e.g.*, Li_2CO_3, and left for crystallization at −20 to 3 °C. The isolated crystals of compounds **1–5** were selected for X-ray and spectroscopy measurements and then vacuum-dried to obtain compounds **6–8**. The synthesis of $LiOH{\cdot}H_2O$ was performed by means of a direct reaction of battery anodes with 60 cm^3 of H_2O. The yield of the lithium recovery from the discharged batteries is calculated based on the initial lithium content in the LMBs.

The cathode material of Li–MnO_2 batteries is generally introduced into a 1000 cm^3 beaker; 100 to 500 cm^3 of distilled water is then added, and the mixture is stirred vigorously for 2–24 hours. The obtained composition is filtered and washed with an additional 500–1500 cm^3 of H_2O and 50 cm^3 of MeOH. The filtrate after evaporation to dryness consists of Li_2CO_3 and $LiClO_4{\cdot}3H_2O$. Next, $LiClO_4{\cdot}3H_2O$ is removed from the resulting mixture by extraction with CH_3OH. The resulting black precipitate of the weight from 20 to 50 g is a mixture of carbon black, graphite, MnO_2, and $Li_xMn_2O_4$, with a carbon content of 10 to 15% by weight. Then, carbon black and graphite are removed from the obtained material by heating it to a temperature of 900 °C, producing a mixture of $LiMn_2O_4$ and Mn_2O_3.

Li–FeS_2 battery recycling procedure

16 post-consumer R03/AAA lithium batteries weighing 120.38 g were opened, and their parts containing the anode with a total weight of 2.96 g were placed in a 1000 cm^3 round-bottom flask. Then, 70 cm^3 of methyl salicylate was introduced under a nitrogen atmosphere, and the reaction was left for 30 minutes. To the reaction mixture cooled with an ice/NaCl bath, 150 cm^3 of EtOH was added and left for 2 h. After this time, 200 cm^3 of EtOH was added to dissolve the resulting lithium aryloxide. The mixture was filtered and left to crystallize at −28 °C. After 24 hours, 78.6 g of crystals of compound **4** were obtained with a yield of 38.7%. The crystals were filtered off and dried under vacuum to obtain 64.8 g of **7** with a yield of 32.7%. A Li concentration in 1 g of the cathode material was 0.07485 g. Detailed information regarding the reaction is included in Table S11.†

$[Li(OAr)(HOMe)_2]$ (1)

Spectroscopic characteristics were included in the previously published study.[38]

$[Li(OAr)(HOAr)]$ (2)

Spectroscopic characteristics were included in the previously published study.[38]

$[Li(OAr)(HOEt)]_2$ (3)

Anal. calcd for $C_{22}H_{30}O_8Li_2$: C, 60.56; H, 6.93. Found: C, 60.60; H, 6.95. ^{1}H NMR (400 MHz, THF-d_8): δ 7.70 (2H, dd, J = 8.0, 1.7 Hz, ArH), 7.06 (2H, m, ArH), 6.65 (2H, d, J = 8.5 Hz, ArH), 6.21 (2H, m, ArH), 4.23 (4H, q, J = 7.1 Hz, CH_2^{OAr}), 3.51 (4H, q, J = 7.0 Hz, CH_2^{EtOH}), 3.37 (2H, s, OH^{EtOH}), 1.30 (6H, t, J = 7.1 Hz, CH_3^{OAr}), 1.09 (6H, t, J = 7.0 Hz, CH_3^{EtOH}). ^{13}C NMR (NMR (101 MHz, THF-d_8): δ 173.99 (2C, C═O), 170.74 (2C, C–O), 134.75 (2C, ArH), 132.15 (2C, ArH), 124.72 (2C, ArH), 115.50 (2C, Ar), 111.68 (2C, ArH), 60.25 (2C, CH_2^{OAr}), 57.80 (2C, CH_2^{EtOH}), 19.03 (2C, CH_3^{EtOH}), 14.76 (2C, CH_3^{OAr})). ^{7}Li NMR (155 MHz, THF-d_8): δ 3.95 (2Li). FTIR-ATR (cm^{-1}): 3321 (m), 2973 (m), 2928 (w), 2893 (w), 1926 (vw), 1674 (s), 1598 (w), 1542 (w), 1466 (m), 1445 (m), 1370 (w), 1317 (m), 1258 (m), 1216 (vs), 1156 (s), 1083 (s), 1046 (vs), 949 (vw), 880 (m), 825 (vw), 799 (vw), 758 (m), 709 (m), 659 (w), 583 (w), 535 (vw), 428 (w).

$[Li(OAr)(H_2O)]_2$ (4)

Anal. calcd for $C_{16}H_{18}O_8Li_2$: C, 54.56; H, 5.15. Found: C, 54.57; H, 5.16. ^{1}H NMR (400 MHz, THF-d_8): δ 7.67 (2H, dd, J = 8.1, 2.0 Hz, ArH), 7.07 (2H, ddd, J = 8.7, 6.8, 2.0 Hz, ArH), 6.60 (2H, dd, J = 8.6, 0.9 Hz, ArH), 6.20 (2H, m, ArH), 3.76 (6H, s, CH_3), 2.75 (4H, s, H_2O). ^{13}C NMR (NMR (101 MHz, THF-d_8): δ 173.98 (2C, C═O), 171.18 (2C, C–O), 134.90 (2C, ArH), 132.14 (2C, ArH), 124.56 (2C, ArH), 114.98 (2C, Ar), 111.59 (2C, ArH), 51.21 (2C, CH_3)). ^{7}Li NMR (155 MHz, THF-d_8): δ 3.96 (2Li). FTIR-ATR (cm^{-1}): 3561 (m), 3335 (w), 3155 (w), 3092 (vw), 3031 (vw), 3002 (vw), 2953 (w), 2851 (vw), 2788 (vw), 2667 (vw), 1756 (w), 1643 (s), 1598 (m), 1541 (s), 1465 (m), 1438 (vs), 1323 (vs), 1261 (m), 1219 (vs), 1195 (vs), 1154 (s), 1142 (s), 1087 (s), 1037 (m), 980 (vw), 963 (vw), 948 (w), 863 (m), 817 (m), 800 (w), 758 (s), 708 (m), 656 (m), 581 (w), 552 (w), 485 (vw), 447 (w).

$[Li_4(OAr)_4(EGME)_2]$ (5)

Anal. calcd for $C_{46}H_{60}O_{20}Li_4$: C, 57.51; H, 6.29. Found: C, 57.54; H, 6.31. ^{1}H NMR (400 MHz, THF-d_8): δ 7.73 (4H, dd, J = 8.1, 1.9 Hz, ArH), 7.08 (4H, ddd, J = 8.7, 6.9, 1.9 Hz, ArH), 6.63 (4H, m, ArH), 6.23 (4H, m, ArH), 4.31 (8H, m, CH_2^{OAr}), 3.75 (2H, s, OH^{EGME}) 3.62 (8H, m, CH_2^{OAr}), 3.54 (4H, t, J = 5.1 Hz, CH_2^{EGME}), 3.36 (4H, t, J = 5.1 Hz, CH_2^{EGME}), 3.32 (12H, s, CH_3^{OAr}), 3.28 (6H, s, CH_3^{EGME}). ^{13}C NMR (NMR (101 MHz, THF-d_8): δ 173.97 (4C, C═O), 170.62 (4C, C–O), 134.93 (4C, ArH), 132.31 (4C, ArH), 124.62 (4C, ArH), 115.25 (4C, Ar), 111.80 (4C, ArH), 75.39 (2C, CH_2^{EGME}), 71.50 (4C, CH_2^{OAr}),

63.73 (4C, CH_2^{OAr}), 62.00 (2C, CH_2^{EGME}), 58.94 (4C, CH_3^{OAr}), 58.84 (2C, CH_3^{EGME})). ^{7}Li NMR (155 MHz, THF-d_8): δ 3.94 (4Li). FTIR-ATR (cm^{-1}): 3414 (w), 3048 (w), 3027 (w), 2943 (w), 2878 (w), 2840 (w), 1645 (vs), 1601 (m), 1537 (m), 1512 (w), 1467 (s), 1454 (s), 1407 (w), 1391 (w), 1373 (m), 1359 (m), 1323 (m), 1257 (m), 1240 (m), 1216 (s), 1198 (m), 1156 (s), 1148 (s), 1129 (m), 1080 (vs), 1029 (m), 973 (m), 951 (w), 899 (m), 889 (m), 857 (m), 842 (m), 830 (m), 813 (m), 795 (w), 762 (m), 709 (m), 660 (m), 598 (m), 578 (m), 535 (w), 489 (w), 462 (w).

[$Li_6(OAr)_6$] (6)

Spectroscopic characteristics were included in the previously published study.[38]

[$Li_6(OAr)_6$] (7)

Anal. calcd for $C_{54}H_{54}O_{18}Li_6$: C, 62.81; H, 5.27. Found: C, 62.83; H, 5.28. ^{1}H NMR (400 MHz, THF-d_8): δ 7.74 (6H, dd, J = 8.1, 2.0 Hz, ArH), 7.10 (6H, ddd, J = 8.7, 6.8, 2.0 Hz, ArH), 6.70 (6H, dd, J = 8.5, 0.8 Hz, ArH), 6.27 (6H, ddd, J = 8.0, 6.9, 1.1 Hz, ArH), 4.24 (12H, q, J = 7.1 Hz, CH_2), 1.32 (18H, t, J = 7.1 Hz, CH_3). ^{13}C NMR (NMR (101 MHz, THF-d_8): δ 173.62 (6C, C═O), 170.68 (6C, C–O), 134.82 (6C, ArH), 132.11 (6C, ArH), 124.69 (6C, ArH), 115.66 (6C, Ar), 112.13 (6C, ArH), 60.39 (6C, CH_2), 14.76 (6C, CH_3)). ^{7}Li NMR (155 MHz, THF-d_8): δ 4.03 (6Li). FTIR-ATR (cm^{-1}): 3057 (vw), 2986 (w), 2906 (w), 2775 (w), 2649 (vw), 1674 (vs), 1598 (m), 1545 (m), 1471 (s), 1444 (s), 1399 (w), 1369 (m), 1332 (s), 1314 (s), 1262 (m), 1222 (vs), 1163 (m), 1149 (m), 1114 (w), 1084 (s), 1042 (w), 1028 (w), 973 (vw), 952 (w), 893 (m), 875 (vw), 861 (m), 820 (m), 796 (w), 760 (vs), 707 (s), 660 (m), 588 (vs), 542 (m), 528 (m), 476 (m), 441 (m), 425 (w).

[$Li_6(OAr)_6$] (8)

Anal. calcd for $C_{60}H_{66}O_{24}Li_6$: C, 59.42; H, 5.49. Found: C, 59.45; H, 5.50. ^{1}H NMR (400 MHz, THF-d_8): δ 7.74 (6H, dd, J = 8.1, 2.0 Hz, ArH), 7.09 (6H, ddd, J = 8.7, 6.8, 2.0 Hz, ArH), 6.65 (6H, dd, J = 8.5, 0.8 Hz, ArH), 6.24 (6H, ddd, J = 8.0, 6.9, 1.1 Hz, ArH), 4.31 (12H, m, CH_2^{OAr}), 3.62 (12H, m, CH_2^{OAr}), 3.32 (18H, s, CH_3^{OAr}). ^{13}C NMR (NMR (101 MHz, THF-d_8): δ 173.83 (6C, C═O), 170.58 (6C, C–O), 134.95 (6C, ArH), 132.30 (6C, ArH), 124.60 (6C, ArH), 115.31 (6C, Ar), 111.95 (6C, ArH), 71.48 (6C, CH_2^{OAr}), 63.77 (6C, CH_2^{OAr}), 58.94 (6C, CH_3^{OAr}); EGME traces: 75.38 (CH_2^{EGME}), 61.99 (CH_2^{EGME}), 58.85 (CH_3^{EGME})). ^{7}Li NMR (155 MHz, THF-d_8): δ 3.95 (6Li). FTIR-ATR (cm^{-1}): 3325 (w), 3054 (vw), 3028 (vw), 2994 (vw), 2944 (m), 2878 (w), 2840 (w), 2767 (vw), 2734 (vw), 2685 (vw), 2578 (vw), 1953 (vw), 1929 (vw), 1900 (vw), 1834 (vw), 1808 (vw), 1645 (vs), 1601 (m), 1537 (m), 1512 (vw), 1467 (vs), 1453 (s), 1407 (vw), 1391 (w), 1373 (m), 1359 (m), 1323 (m), 1257 (m), 1216 (vs), 1199 (m), 1156 (vs), 1148 (s), 1130 (m), 1081 (vs), 1030 (m), 972 (w), 951 (vw), 899 (w), 890 (m), 858 (m), 843 (vw), 813 (w), 795 (vw), 762 (vs), 709 (s), 660 (m), 599 (s), 581 (s), 549 (w), 535 (w), 489 (w), 436 (w).

[$Li_6(OAr)_6(EGME)_2$] (8·2EGME)

Anal. calcd for $C_{66}H_{82}O_{28}Li_6$: C, 58.07; H, 6.06. Found: C, 58.11; H, 6.09. ^{1}H NMR (400 MHz, THF-d_8): δ 7.72 (6H, dd, J = 8.1, 1.8 Hz, ArH), 7.07 (6H, ddd, J = 8.6, 6.9, 1.9 Hz, ArH), 6.64 (6H, m, ArH), 6.22 (6H, m, ArH), 4.30 (12H, m, CH_2^{OAr}), 3.66 (2H, s, OH^{EGME}), 3.61 (12H, m, CH_2^{OAr}), 3.55 (4H, t, J = 5.1 Hz, CH_2^{EGME}), 3.36 (4H, t, J = 5.1 Hz, CH_2^{EGME}), 3.32 (18H, s, CH_3^{OAr}), 3.28 (6H, s, CH_3^{EGME}). ^{13}C NMR (101 MHz, THF-d_8): δ 174.03 (6C, C═O), 170.63 (6C, C–O), 134.91 (6C, ArH), 132.30 (6C, ArH), 124.70 (6C, ArH), 115.31 (6C, Ar), 111.77 (6C, ArH), 75.39 (2C, CH_2^{EGME}), 71.51 (6C, CH_2^{OAr}), 63.73 (6C, CH_2^{OAr}), 62.01 (2C, CH_2^{EGME}), 58.94 (6C, CH_3^{OAr}), 58.85 (2C, CH_3^{EGME}). ^{7}Li NMR (155 MHz, THF-d_8): δ 3.97 (6Li). FTIR-ATR (cm^{-1}): 3373 (w), 3049 (w), 3027 (w), 2943 (w), 2878 (w), 2840 (w), 1645 (vs), 1601 (m), 1537 (m), 1512 (w), 1483 (m), 1467 (m), 1453 (m), 1407 (w), 1391 (w), 1373 (m), 1359 (m), 1323 (m), 1257 (m), 1239 (m), 1216 (s), 1198 (m), 1157 (s), 1148 (s), 1129 (m), 1081 (vs), 1029 (m), 972 (m), 951 (w), 899 (m), 890 (m), 857 (m), 843 (m), 830 (m), 813 (m), 795 (w), 762 (s), 709 (m), 660 (m), 598 (m), 581 (m), 535 (m), 490 (w), 462 (w).

Author contributions

Rafał Petrus: conceptualization, investigation, project administration, funding acquisition, writing – original draft, and writing – review, and editing. Adrian Kowaliński: NMR and IR investigation of **5–8** and analytical and PXRD investigation of cathode materials. Tadeusz Lis: single-crystal X-ray diffraction measurements. All authors have read and approved the final version of the manuscript.

Conflicts of interest

There are no conflicts to declare.

Acknowledgements

We gratefully acknowledge the financial support obtained from the Polish National Science Center, grant no. 2017/26/D/ST5/01123 (RP). The work was also co-financed by a statutory activity subsidy from the Polish Ministry of Science and Education for the Faculty of Chemistry of Wrocław University of Science and Technology (AK). The authors would like to thank Dr Józef Utko for his help in the crystallization of compounds **5** and **9**.

Notes and references

1 K. Chapman, The lithium rush, https://www.chemistryworld.com/features/the-lithium-rush/4017304.article, accessed 2023-10-17.
2 M. J. Akbar, Lithium Reserves by Country: Top 5 Countries, https://www.insidermonkey.com/blog/lithium-

reserves-by-country-top-5-countries-1157105/; Lithium Reserves by Country: Top 15 Countries, https://www.insidermonkey.com/blog/lithium-reserves-by-country-top-15-countries-1157106/, accessed 2023-10-17.

3 L. Baudino, C. Santos, C. F. Pirri, F. La Mantia and A. Lamberti, Recent Advances in the Lithium Recovery from Water Resources: From Passive to Electrochemical Methods, *Adv. Sci.*, 2022, **9**, 2201380.

4 Z. J. Baum, R. E. Bird, X. Yu and J. Ma, Lithium-Ion Battery Recycling—Overview of Techniques and Trends, *ACS Energy Lett.*, 2022, **7**, 712–719.

5 X. Zhang, L. Li, E. Fan, Q. Xue, Y. Bian, F. Wu and R. Chen, Toward sustainable and systematic recycling of spent rechargeable batteries, *Chem. Soc. Rev.*, 2018, **47**, 7239–7302.

6 J. Neumann, M. Petrániková, M. Meeus, J. D. Gamarra, R. Younesi, M. Winter and S. Nowak, Recycling of Lithium-Ion Batteries—Current State of the Art, Circular Economy, and Next Generation Recycling, *Adv. Energy Mater.*, 2022, **12**, 2102917.

7 W. McLaughlin and T. S. Adams, Li reclamation process, US5888463A, 1999, (Application number US09/002,434).

8 F. Tedjar and J.-C. Foudraz, Method for the mixed recycling of lithium-based anode batteries and cells, US7820317B2, 2010, (Application number US10/593,332); W. McLaughlin and T. S. Adams, Li reclamation process, US5888463A, 1999, (Application number US09/002,434).

9 T. Wellera and M. Tenzera, Utilization of lithium battery, CN106058349A, 2016, (Application number CN201610208592.5A).

10 S. Kawakami, Verfahren zur Werkstoffrückgewinnung von Lithiumzellen, EP0613198B1, 1999, (Application number EP19940102823).

11 Z. Zhanyi, C. Kanga, Z. Zhiyonha, L. Congyu, W. Weia and C. Xiaocong, A kind of recovery method of anode material of lithium battery, CN104143668B, 2017, (Application number CN201310532433.7A).

12 S. Joo, S. M. Shin, D. Shin and J.-P. Wang, Development of recycling technology to recover valuable metals from lithium primary and ion batteries, *Proc. Inst. Mech. Eng., Part B*, 2015, **229**, 212–220.

13 M. Contestabile, S. Panero and B. Scrosati, A laboratory-scale lithium battery recycling process, *J. Power Sources*, 2001, **92**, 65–69.

14 A. Boyko, V. Krasilnikov, V. Tagaev, E. Potoropin and B. Serebrennikov, Method of recycling expired lithium cells, RU2531911C1, 2014, (Application number RU2013154384/07A).

15 M. Nisula, J. Linnera, A. J. Karttunen and M. Karppinen, Lithium Aryloxide Thin Films with Guest-Induced Structural Transformation by ALD/MLD, *Chem. – Eur. J.*, 2017, **23**, 2988–2992.

16 K. M. Fromm, A. Crochet and J.-P. Brog, Lithium metal aryloxide clusters as starting products for oxide materials, WO2012000123A1, 2012, (Application number PCT/CH2011/000149).

17 B. T. Zhang, A. J. Easteal, N. R. Edmonds and D. Bhattacharyya, Sol–gel preparation and characterization of lithium disilicate glass–ceramic, *J. Am. Ceram. Soc.*, 2007, **90**, 1592–1596.

18 W. Ranus, R. Loewenstein, F. Weiberth, J. Zirlis and H. Bugbee, Carboxylierung von Metallaryloxiden, EP0102833A1, 1986, (Application number EP83305055A).

19 E. Staude and A. Hussain, The Lithium Phenoxide Catalyzed Addition of Propylene Oxide to Phenol, *Polym. J.*, 1971, **2**, 468–474.

20 R. Petrus, J. Utko, R. Gniłka, M. G. Fleszar, T. Lis and P. Sobota, Solvothermal Alcoholysis Method for Recycling High-Consistency Silicone Rubber Waste, *Macromolecules*, 2021, **54**, 2449–2465.

21 M. K. Bisai, K. Gour, T. Das, K. Vanka and S. S. Sen, Readily available lithium compounds as catalysts for the hydroboration of carbodiimides and esters, *J. Organomet. Chem.*, 2021, **949**, 121924.

22 N. Ikpo, C. Hoffmann, L. N. Dawe and F. M. Kerton, Ring-opening polymerization of ε-caprolactone by lithium piperazinyl-aminephenolate complexes: synthesis, characterization and kinetic studies, *Dalton Trans.*, 2012, **41**, 6651–6660.

23 W. Lu, H.-W. Ou, C.-N. Lee, J. K. Vandavasi, C. Y. Li and C. Lin, Synthesis, characterization, and catalytic activity of lithium complexes bearing NNO-tridentate Schiff base ligands toward ring-opening polymerization of L-lactide, *Polymer*, 2018, **139**, 1–10.

24 R. K. Dean, A. M. Reckling, H. Chen, L. N. Dawe, C. J. Schneider and C. M. Kozak, Ring-opening polymerization of cyclic esters with lithium amine-bis(phenolate) complexes, *Dalton Trans.*, 2013, **42**, 3504–3520.

25 D. Alhashmialameer, N. Ikpo, J. Collins, L. N. Dawe, K. Hattenhauer and F. M. Kerton, Ring-opening polymerization of rac-lactide mediated by tetrametallic lithium and sodium diamino-bis(phenolate) complexes, *Dalton Trans.*, 2015, **44**, 20216–20231.

26 H.-Y. Chen, L. Mialon, K. A. Abboud and S. A. Miller, Comparative Study of Lactide Polymerization with Lithium, Sodium, Magnesium, and Calcium Complexes of BHT, *Organometallics*, 2012, **31**, 5252–5261.

27 O. Santoro, M. R. J. Elsegood, S. J. Teat, T. Yamato and C. Redshaw, Lithium calix[4]arenes: structural studies and use in the ring opening polymerization of cyclic esters, *RSC Adv.*, 2021, **11**, 11304–11317.

28 S.-C. Roșca, D. Roșca, V. Dorcet, C. M. Kozak, F. M. Kerton, J. Carpentier and Y. Sarazin, Alkali aminoether-phenolate complexes: synthesis, structural characterization and evidence for an activated monomer ROP mechanism, *Dalton Trans.*, 2013, **42**, 9361–9375.

29 N. Tsubokawa, Y. Nagano and Y. Sone, Grafting of poly-β-alanine from carbon black, *J. Appl. Polym. Sci.*, 1984, **29**, 985–993.

30 C. Schmitz, H. Schmidt and M. Thelakkat, Lithium–Quinolate Complexes as Emitter and Interface Materials in Organic Light-Emitting Diodes, *Chem. Mater.*, 2000, **12**, 3012–3019.

31 H. Wang, B. Xu, X. Liu, H. Zhou, Y. Hao, H. Xu and L. Chen, A novel blue-light organic electroluminescence material derived from 8-hydroxyquinoline lithium, *Org. Electron.*, 2009, **10**, 918–924.
32 J. Kido and T. Matsumoto, Bright organic electroluminescent devices having a metal-doped electron-injecting layer, *Appl. Phys. Lett.*, 1998, **73**, 2866–2868.
33 Y. Pu, M. Miyamoto, K. I. Nakayama, T. Oyama, M. Yokoyama and J. Kido, Lithium phenolate complexes for an electron injection layer in organic light-emitting diodes, *Org. Electron.*, 2009, **10**, 228–232.
34 S. Ohisa, T. Karasawa, Y. Watanabe, T. Ohsawa, Y. Pu, T. Koganezawa, H. Sasabe and J. Kido, A Series of lithium pyridyl phenolate complexes with a pendant pyridyl group for electron-injection layers in organic light-emitting devices, *ACS Appl. Mater. Interfaces*, 2017, **9**, 40541–40548.
35 S. Miles, Methyl Salicylate, *XPharm: The Comprehensive Pharmacology Reference*, 2008, pp. 1–6.
36 D. Jacobsen and K. E. McMartin, in *Alcohols and glycols in Human Toxicology*, ed. J. Descotes, Elsevier Science B.V., 1996, ch. 24, pp. 623–648.
37 Information taken from product safety data sheet from manufacturers' websites.
38 R. Petrus, P. Fałat and P. Sobota, Use of lithium aryloxides as promoters for preparation of α-hydroxy acid esters, *Dalton Trans.*, 2020, **49**, 866–876.
39 T. A. Hanna, L. Liu, A. M. Ángeles-Boza, X. Kou, C. D. Gutsche, K. Ejsmont, W. H. Watson, L. N. Zakharov, C. D. Incarvito and A. L. Rheingold, Synthesis, Structures, and Conformational Characteristics of Calixarene Monoanions and Dianions, *J. Am. Chem. Soc.*, 2003, **125**, 6228–6238.
40 D. M. Cousins, M. G. Davidson, D. García-Vivó and M. F. Mahon, Structural diversity in polyamine Lewis base stabilised lithium aryloxides, *Dalton Trans.*, 2010, **39**, 8203–8209.
41 M.-L. Hsueh, B.-H. Huang, J. Wu and C. Lin, Synthesis, characterization, and catalytic studies of lithium complexes: efficient initiators for ring-opening polymerization of L-lactide, *Macromolecules*, 2005, **38**, 9482–9487.
42 L. Wang, X. Pan, L. Yao, N. Tang and J. Wu, Ring-opening polymerization of L-lactides catalyzed by zinc–sodium/lithium heterobimetallic complexes in the presence of water, *Eur. J. Inorg. Chem.*, 2011, 632–636.
43 C. A. Huang and C. Chen, Lithium complexes supported by amine bis-phenolate ligands as efficient catalysts for ring-opening polymerization of L-lactide, *Dalton Trans.*, 2007, 5561–5566.
44 T. Watanabe, Y. Ishida, T. Matsuo and H. Kawaguchi, Syntheses and structures of zirconium(IV) complexes supported by 2,6-di-adamantylaryloxide ligands and formation of arene-bridged dizirconium complexes with an inverse sandwich structure, *Dalton Trans.*, 2010, **39**, 484–491.
45 T. Matsuo and H. Kawaguchi, Anisole–diphenoxide ligands and their zirconium dichloride and dialkyl complexes, *Inorg. Chem.*, 2007, **46**, 8426–8434.
46 B. Çetınkaya, I. Gumrukcu, M. F. Läppert, J. L. Atwood and R. Shakir, Lithium and sodium 2,6-di-tert-butylphenoxides and the crystal and molecular structure of $[Li(OC_6H_2Me\text{-}4\text{-}Bu^t_2\text{-}2,6)(OEt_2)]_2$, *J. Am. Chem. Soc.*, 1980, **102**, 2086–2088.
47 W. Clegg, E. Lamb, S. T. Liddle, R. Snaith and A. E. H. Wheatley, Towards an understanding of the conjugate addition of organolithium reagents to α,β-unsaturated ketones: the isolation and solid-state structure of a monomeric lithium aluminate with very short agostic Li···HC interactions, *J. Organomet. Chem.*, 1999, **573**, 305–312.
48 J. C. Huffman, R. L. Geerts and K. G. Caulton, Aggregation and solvation of a lithium aryloxide, *J. Crystallogr. Spectrosc. Res.*, 1984, **14**, 541–547.
49 G. Kociok-Köhn, J. Pickardt and H. Schumann, Structure of dimeric lithium 2,6-di-tert-butylphenoxide-diethyl ether, *Acta Crystallogr., Sect. C: Cryst. Struct. Commun.*, 1991, **47**, 2649–2651.
50 M. L. Cole, P. C. Junk, K. M. Proctor, J. L. Scott and C. Strauss, Synthesis and structural characterisation of lithium and sodium 2,6-dibenzylphenolate complexes, *Dalton Trans.*, 2006, 3338–3349.
51 L. Matilainen, M. Klinga and M. Leskelä, Synthesis and X-ray crystal structure of di-μ-(2,6-di-tert-butylphenoxo)dilithium bis-dimethylsulphoxide solvate, $C_{32}H_{54}Li_2O_4S_2$. Comparison of the structure with other dimeric lithium alkoxides, *Polyhedron*, 1995, **14**, 635–638.
52 R. H. Howard, C. Alonso-Moreno, L. M. Broomfield, D. L. Hughes, J. A. Wright and M. Bochmann, Synthesis and structures of complexes with axially chiral isoquinolinyl-naphtholate ligands, *Dalton Trans.*, 2009, 8667–8682.
53 S. Kanazawa, T. Ohira, S. Goda, N. Hayakawa, T. Tanikawa, D. Hashizume, Y. Ishida, H. Kawaguchi and T. Matsuo, Synthesis and Structural Characterization of Lithium and Titanium Complexes Bearing a Bulky Aryloxide Ligand Based on a Rigid Fused-Ring s-Hydrindacene Skeleton, *Inorg. Chem.*, 2016, **55**, 6643–6652.
54 H. Yao, J. Zhang, Y. Zhang, H. Sun and Q. Shen, Synthesis of Cationic N-Heterocyclic Carbene Lanthanide Bromide and the Influence of N-Heterocyclic Carbene and Lanthanide Metals, *Organometallics*, 2010, **29**, 5841–5846.
55 C. A. Huang, C.-L. Ho and C. Chen, Structural and catalytic studies of lithium complexes bearing pendant aminophenolate ligands, *Dalton Trans.*, 2008, 3502–3510.
56 H. Shere, P. McKeown, M. F. Mahon and M. D. Jones, Making the cut: Monopyrrolidine-based complexes for the ROP of lactide, *Eur. Polym. J.*, 2019, **114**, 319–325.
57 Y. Zhou, G. S. Nichol and J. A. Garden, Lithium Half-Salen Complexes: Synthesis, Structural Characterization and Studies as Catalysts for rac-Lactide Ring-Opening Polymerization, *Eur. J. Org. Chem.*, 2021, 5557–5568.
58 F. M. García-Valle, R. Estivill, C. Gallegos, T. Cuenca, M. E. G. Mosquera, V. Tabernero and J. Cano, Metal and Ligand-Substituent Effects in the Immortal Polymerization of rac-Lactide with Li, Na, and K Phenoxo-imine Complexes, *Organometallics*, 2015, **34**, 477–487.

59 S. K. Ghosh, D. Chakraborty and B. Varghese, Group 1 salts of the imino(phenoxide) scaffold: Synthesis, structural characterization and studies as catalysts towards the bulk ring opening polymerization of lactides, *Eur. Polym. J.*, 2015, **62**, 51–65.
60 T. Rosén, K. Kirschbaum and D. M. Giolando, Solid state and solution structures of 2-halophenolate complexes of lithium, *Inorg. Chim. Acta*, 2005, **358**, 3680–3690.
61 J. M. Harrowfield, B. W. Skelton and A. H. White, Structural Studies of the Alkali Metal Picrates, *Aust. J. Chem.*, 1995, **48**, 1311–1331.
62 A. Budanow, M. Bolte and M. Wagner, CSD Communication, 2022, (refcode BECQOT).
63 P. A. Slepukhin, N. S. Boltacheva, V. I. Filyakova and V. N. Charushin, Synthesis and structure of lithium 3-trifluoromethyl-1,3-diketonates containing pyridyl substituents, *Russ. Chem. Bull.*, 2019, **68**, 1213–1218.
64 M. Pinsky and D. Avnir, Continuous Symmetry Measures. 5. The Classical Polyhedra, *Inorg. Chem.*, 1998, **37**, 5575–5582.
65 D. Waldmüller, B. Mayer, M. Braun, A. Hanuschik, C. Krüger and P. Guénot, Kristallstruktur und Gasphasenuntersuchungen von lithiiertem Acetessigsäure-tert-butylester, *Chem. Ber.*, 1992, **125**, 2779–2782.
66 C. Frenzel and E. Hey-Hawkins, Benzophenone Oxidation of Primary Lithium Phosphanides to Cyclooligophosphanes With Formation of Lithium Diphenylmethanolate, *Phosphorus, Sulfur Silicon Relat. Elem.*, 1998, **143**, 1–17.
67 N. Meyer, R. Rüttinger and P. W. Roesky, Lithium and Ytterbium Aminotroponate Complexes, *Eur. J. Inorg. Chem.*, 2008, 1830–1833.
68 M. A. Nichols, C. M. Leposa, A. D. Hunter and M. Zeller, Crystal Structures of Hexameric and Dimeric Complexes of Lithioisobutyrophenone, *J. Chem. Crystallogr.*, 2007, **37**, 825–829.
69 B. Goldfuß, P. Von Ragué Schleyer and F. Hampel, A "Lithium-Bonded" Cyclopropyl Edge: The X-ray Crystal Structure of $[Li–O–C(Me)–(c\text{-}CHCH_2CH_2)_2]_6$ and Computational Studies, *J. Am. Chem. Soc.*, 1996, **118**, 12183–12189.
70 C. Strohmann, T. Seibel and D. Schildbach, (2S)-1-Methyl-2-(oxymethyl)pyrrolidine, The Crystal Structures of a Chiral Aminoalkoxide Cluster and Its Adduct with Benzyllithium, *J. Am. Chem. Soc.*, 2004, **126**, 9876–9877.
71 B. Goldfuß, P. Von Ragué Schleyer and F. Hampel, Alkali Metal Cation π-Interactions in Metalated and Nonmetalated Acetylenes: π-Bonded Lithiums in the X-ray Crystal Structures of $[Li–C{:}C–SiMe_2–C_6H_4–OMe]_6$ and $[Li–O–CMe_2–C{:}C–H]_6$ and Computational Studies, *J. Am. Chem. Soc.*, 1997, **119**, 1072–1080.
72 G. Müller and A. Feustel, Multidentate Phosphinoalkoxides: Synthesis, Deprotonation, and Building Blocks in Polylithium Mixed-Anion Aggregates, *Organometallics*, 2003, **22**, 3049–3058.
73 B. Goldfuß, P. Von Ragué Schleyer and F. Hampel, "Lithio-Aversion" of Thiophene Sulfur Atoms in the X-ray Crystal Structures of $[Li–O–SiMe_2(2\text{-}C_4H_3S)]_6$ and $[Li–O–CH(i\text{-}Pr)(2\text{-}C_4H_3S)]_6$: Models for Electrostatic Metal–Thiophene Interactions, *Organometallics*, 1997, **16**, 5032–5041.
74 M. H. Chisholm, S. R. Drake, A. A. Naiini and W. E. Streib, The synthesis and characterization of volatile lithium alkoxides, and the single crystal X-ray structure of $[LiOCMe_2Ph]_6$, *Polyhedron*, 1991, **10**, 805–810.
75 M. Iwasaki, T. Narita and Y. Umino, On the structure of lithium 2-(1-pyrrolidyl)ethoxide with benzyllithium, *J. Organomet. Chem.*, 2011, **696**, 2763–2766.
76 A. J. McNeil, G. E. S. Toombes, S. V. Chandramouli, B. Vanasse, T. A. Ayers, M. K. O'Brien, E. Lobkovsky, S. M. Grüner, J. A. Marohn and D. B. Collum, Characterization of β-Amino Ester Enolates as Hexamers via ^{6}Li NMR Spectroscopy, *J. Am. Chem. Soc.*, 2004, **126**, 5938–5939.
77 P. G. Williard and G. B. Carpenter, X-ray crystal structure of an unsolvated lithium enolate anion, *J. Am. Chem. Soc.*, 1985, **107**, 3345–3346.
78 M. T. Muñoz, C. Urbaneja, M. Temprado, M. E. G. Mosquera and T. Cuenca, Lewis acid fragmentation of a lithium aryloxide cage: generation of new heterometallic aluminium–lithium species, *Chem. Commun.*, 2011, **47**, 11757–11759.
79 A. Bodach, J. Ortmeyer, B. Herrmann and M. Felderhoff, Amino-Organolithium Compounds and their Aggregation for the Synthesis of Amino-Organoaluminium Compounds, *Eur. J. Inorg. Chem.*, 2021, 2248–2256.
80 M. Rajeswaran, W. J. Begley, L. P. Olson and S. Huo, Steric effects of substituted quinolines on lithium coordination geometry, *Polyhedron*, 2007, **26**, 3653–3660.
81 A. W. Brzeczko, R. Leech and J. G. Stark, The advent of a new pseudoephedrine product to combat methamphetamine abuse, *Am. J. Drug Alcohol Abuse*, 2013, **39**, 284–290.
82 R. Plumstead, Incorporating lithium salicylate or the like into a grease, US3711407A, 1990, (Application number US00090878A).
83 A. J. De Smith, S.-H. Kim, J. Tan, K. B. Sneed, P. R. Sanberg, C. V. Borlongan and R. D. Shytle, Plasma and Brain Pharmacokinetics of Previously Unexplored Lithium Salts, *RSC Adv.*, 2014, **4**, 12362–12365.
84 N. Zaitseva, J. Newby, G. Hull, C. K. Saw, L. Carman, N. J. Cherepy and S. A. Payne, Growth and Properties of Lithium Salicylate Single Crystals, *Cryst. Growth Des.*, 2009, **9**, 3799–3802.
85 F. Wiesbrock and H. Schmidbaur, Lithium salicylate monohydrate: A layer structure with carboxylate-bridged Δ- and Λ-$[(H_2O)Li^+]_\infty$ helices, *CrystEngComm*, 2003, **5**, 503–505.
86 V. M. Tran and M. L. P. Le, Capacitance behavior of nanostructured ε-MnO_2/C composite electrode using different carbons matrix, *Adv. Nat. Sci.: Nanosci. Nanotechnol.*, 2014, **5**, 025005.
87 W. M. Dose and S. W. Donne, Thermal Treatment Effects on Manganese Dioxide Structure, Morphology and

Electrochemical Performance, *J. Electrochem. Soc.*, 2011, **158**, A905.

88 W. Liu, T. S. Yu, Z. Dai, M. Zhang, H. Jin, H. Ge, X. Wang, D. Jin and H. Liu, Facile Preparation of High Performance Low Concentration HCHO Degradation Catalyst from Waste Li-MnO_2 Batteries, *J. Inorg. Organomet. Polym. Mater.*, 2023, **33**, 451–461.

89 W. I. F. David, M. M. Thackeray, P. G. Bruce and J. B. Goodenough, Lithium insertion into β MnO_2 and the rutile-spinel transformation, *Mater. Res. Bull.*, 1984, **19**, 99–106.

90 Y. Shao-Horn, S. A. Hackney and B. C. Cornilsen, Structural Characterization of Heat-treated Electrolytic Manganese Dioxide and Topotactic Transformation of Discharge Products in the Li–MnO_2 Cells, *J. Electrochem. Soc.*, 1997, **144**, 3147–3153.

91 K. Yamaura, Q. Huang, L. Zhang, K. Takada, Y. Baba, T. Nagai, Y. Matsui, K. Kosuda and E. Takayama-Muromachi, Spinel-to-$CaFe_2O_4$-Type Structural Transformation in $LiMn_2O_4$ under High Pressure, *J. Am. Chem. Soc.*, 2006, **128**, 9448–9456.

92 H. Tan, S. Wang and X. Lei, New Insights for the Cyclic Performance of Li/MnO_2 Batteries Using a Simple Electrochemical Process, *J. Electrochem. Soc.*, 2015, **162**, A448–A452.

93 M. H. Brooker and J. B. Bates, Raman and Infrared Spectral Studies of Anhydrous Li_2CO_3 and Na_2CO_3, *J. Chem. Phys.*, 1971, **54**, 4788–4796.

94 S. I. Ivlev, D. V. Akimov, N. B. Egorov and F. Kraus, Synthesis and characterization of $LiClO_4 \cdot H_2O$, *Monatsh. Chem.*, 2015, **147**, 279–288.

95 M. Takeuchi, R. Kurosawa, J. Ryu and M. Matsuoka, Hydration of LiOH and LiCl—Near-Infrared Spectroscopic Analysis, *ACS Omega*, 2021, **6**, 33075–33084.

96 J. F. L. Silva, M. C. Policano, G. C. Tonon, C. G. Anchieta, G. Doubek and R. M. Filho, The potential of hydrophobic membranes in enabling the operation of lithium-air batteries with ambient air, *Chem. Eng. J. Adv.*, 2022, **11**, 100336.

97 S.-F. Wang, Y.-L. Liao, Y. Hsu and P. Jasiński, Effects of Ni-NCAL and Ni–Ag electrodes on the cell performances of low-temperature solid oxide fuel cells with $Sm_{0.2}Ce_{0.8}O_{2-\delta}$ electrolyte at various temperatures, *Int. J. Hydrogen Energy*, 2022, **47**, 40067–40082.

98 N. R. Lobanov, Production of intensive negative lithium beam with caesium sputter-type ion source, *Nucl. Instrum. Methods Phys. Res., Sect. B*, 2018, **415**, 72–81.

99 F. S. Gittleson, K. P. C. Yao, D. G. Kwabi, S. Y. Sayed, W. Ryu, Y. Shao-Horn and A. D. Taylor, Raman Spectroscopy in Lithium–Oxygen Battery Systems, *ChemElectroChem*, 2015, **2**, 1446–1457.

100 E. Di Pietro, M. Pagliai, G. Cardini and V. Schettino, Solid-state phase transition induced by pressure in $LiOH \times H_2O$, *J. Phys. Chem. B*, 2006, **110**, 13539–13546.

101 V. I. Tyutyunnik, Lithium hydroxide monohydrate single crystals: infrared reflectivity and Raman study, *J. Raman Spectrosc.*, 2000, **31**, 559–563.

102 M. Rivlin, U. Eliav and G. Navon, NMR Studies of the Equilibria and Reaction Rates in Aqueous Solutions of Formaldehyde, *J. Phys. Chem. B*, 2015, **119**, 4479–4487.

103 S. Freunberger, Y. Chen, Z. Peng, J. M. Griffin, L. J. Hardwick, F. Bardé, P. Novák and P. G. Bruce, Reactions in the Rechargeable Lithium–O_2 Battery with Alkyl Carbonate Electrolytes, *J. Am. Chem. Soc.*, 2011, **133**, 8040–8047.

104 W. Kwak, Rosy, D. Sharon, C. Xia, H. Kim, L. Johnson, P. G. Bruce, L. F. Nazar, Y. K. Sun, A. A. Frimer, M. Noked, S. Freunberger and D. Aurbach, Lithium-Oxygen Batteries and Related Systems: Potential, Status, and Future, *Chem. Rev.*, 2020, **120**, 6626–6683.

105 P. Strobel, F. L. Cras, L. Seguin, M. Anne and J. Tarascon, Oxygen Nonstoichiometry in Li–Mn–O Spinel Oxides: A Powder Neutron Diffraction Study, *J. Solid State Chem.*, 1998, **135**, 132–139.

106 A. Mosbah, A. Verbaere and M. Tournoux, Phases $Li_xMnO_2\lambda$ rattachees au type spinelle, *Mater. Res. Bull.*, 1983, **18**, 1375–1381.

107 X. Tan, J. Zhao, M. Jiang, S. Nie, Y. Li, X. Wang, Y. Wang, X. Kang, H. Wang and W. Chu, Different roles of oxygen deficiency in performance of spinel lithium manganese oxides as the cathodes for aqueous and non-aqueous systems, *Ionics*, 2021, **27**, 4249–4257.

108 *Agilent, CrysAlis PRO*, Agilent Technologies Ltd, Yarnton, Oxfordshire, England, 2014.

109 G. M. Sheldrick, Crystal Structure Refinement with SHELXL, *Acta Crystallogr., Sect. C: Struct. Chem.*, 2015, **71**, 3–8.

110 K. Brandenburg, *Diamond*, Crystal Impact GbR, Bonn, Germany, 2007.